LBNL-39572
UC-412
Preprint

ERNEST ORLANDO LAWRENCE BERKELEY NATIONAL LABORATORY

Orbital Tuning of Paleoclimatic Records: A Reassessment

Binyamin U. Neeman
Physics Division

April 1993
Submitted to
Journal of Climate

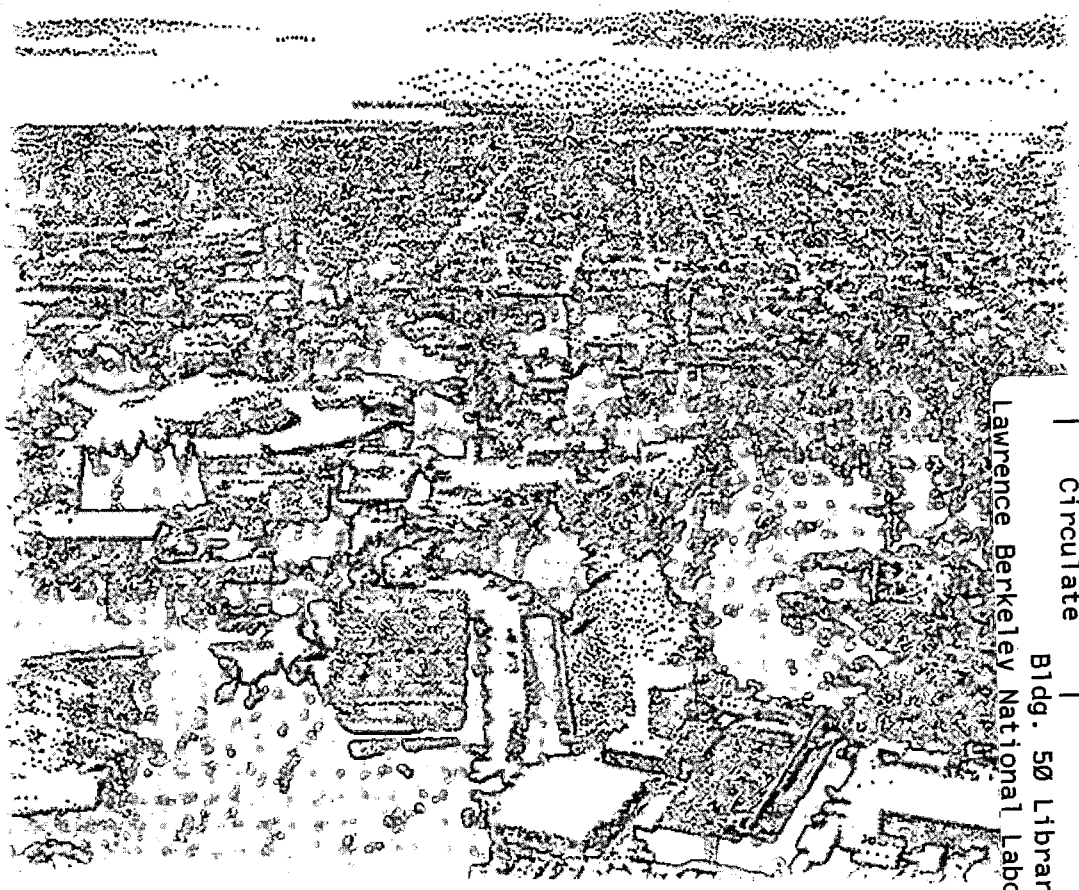

REFERENCE COPY
Does Not
Circulate
Bldg. 50 Library - Ref.
Lawrence Berkeley National Laboratory
Copy 1
LBNL-39572

DISCLAIMER

This document was prepared as an account of work sponsored by the United States Government. While this document is believed to contain correct information, neither the United States Government nor any agency thereof, nor the Regents of the University of California, nor any of their employees, makes any warranty, express or implied, or assumes any legal responsibility for the accuracy, completeness, or usefulness of any information, apparatus, product, or process disclosed, or represents that its use would not infringe privately owned rights. Reference herein to any specific commercial product, process, or service by its trade name, trademark, manufacturer, or otherwise, does not necessarily constitute or imply its endorsement, recommendation, or favoring by the United States Government or any agency thereof, or the Regents of the University of California. The views and opinions of authors expressed herein do not necessarily state or reflect those of the United States Government or any agency thereof or the Regents of the University of California.

LBNL-39572
UC-412

Orbital Tuning of Paleoclimatic Records: A Reassessment

Binyamin U. Neeman

Department of Geophysics and Planetary Sciences
Raymond and Sackler Faculty of Exact Sciences
Tel Aviv University
Tel Aviv 69978, Israel

April 1993

This work was printed by Lawrence Berkeley National Laboratory, which is funded by the U.S. Department of Energy under Contract No. DE-AC03-76SF00098.

Orbital Tuning of Paleoclimatic Records: a Reassessment

Binyamin U. Neeman

Department of Geophysics and Planetary Sciences, Raymond and Sackler Faculty of Exact Sciences,

Tel Aviv University, Tel Aviv 69978, Israel

April 1993

(Submitted to Journal of Climate)

(Revised, July 1994)

ABSTRACT

A computer program is developed for tuning paleoclimatic curves to match the orbital signals of obliquity, precession and eccentricity or their combination. The tuning consists of clicking a control point and pulling it along the time axis. The software has graphic and mathematical capabilities to perform a real-time orbital tuning displaying the resulting power spectrum and coherence function while the curve is being tuned. A random curve is orbitally tuned within the range of constrictions common in other marine chronostratigraphic studies. Results show that coherencies above 0.9 in the precessional and obliquity orbital bands and near the 100 Kyr eccentricity period may be achieved simultaneously as an artifact of the orbital tuning. Furthermore, the solution of orbital tuning is non-unique. This example is a vivid proof that orbital tuning cannot be the basis of any support for the orbital theory, nor can it be used for quantitative estimates of the portion of orbital forcing. The 100 Kyr peak obtained by orbitally tuning paleoclimatic records to obliquity and precession should not be linked with eccentricity since coherence in the overall eccentricity band remains low, and since this phenomenon was also observed tuning a random curve. Analysis of the V28-238 $\delta^{18}O$ record before orbital tuning shows peaks in the power spectrum near orbital periods, which may either be coincidental or represent the blurred contribution of orbital forcing. By artificially removing these peaks, it is illustrated that this contribution is negligible. Tuning the V28-238 $\delta^{18}O$ record to a previously published independent time scale based on constant aluminum accumulation and anchored by 11 ^{230}Th dates shows even less similarity with the orbital signal.

1. Background

A consensus exists today among marine chronostratigraphers that paleoclimatic records from deep-sea sediment cores vary with periodicities that match those of the earth's orbital variations (e.g. Hays et al., 1976; Imbrie et al., 1984; Martinson et al., 1987; and others). However, in order to obtain this match, it was necessary to calibrate the depth-in-core with time by the method of orbital tuning. Orbital tuning is an iterative process by which each excursion in the paleoclimatic curve being tuned is compared with a corresponding excursion in an orbital target curve; and if differences occur, an appropriate adjustment is made in the age of one or more control points. The target curve consists of a high latitude summer solar radiation curve (Milankovitch, 1941) or individual phase-shifted orbital signals. Sometimes digital filters are applied so that the comparison at each step of the iteration is done either in the precession band alone or in the obliquity band alone. Martinson et al. (1982, 1987) used an algorithm which iteratively changes the coefficients of an expansion of the mapping function between the depth in core and time in an orbital target curve.

The justification for orbital tuning is based on a list of effects which blur and smooth the isotopic signal, broadening its spectral peaks and even introducing spurious peaks (Pestiaux and Berger, 1984). Among these effects are changes in the sedimentation rate; sediment transport; bioturbation - the mixing of the top layer of sediments by bottom dwelling organisms; vital and ecological effects; influence by ambient water temperature; changes in evaporation-precipitation rate; stratigraphic disturbances and distortions due to the coring process itself. Orbital tuning is intended to recover the orbital information in the isotopic record by modifying its time calibration.

Hays et al. (1976) orbitally tuned a composite record of oxygen isotope ratio ($\delta^{18}O$) from two deep-sea sediment cores (RC11-120 and E49-18). The records of the two cores were joined at termination III and tuned at termination II, III and V. Hays et al. concluded that 10, 25 and 50% of the variance correspond to precession, obliquity and eccentricity, respectively.

However, Evans and Freeland (1977) interpreted the results of their orbitally tuned age model as indicating that "there may be an astronomical effect, but it is evidently small".

Johnson (1982) suggested orbital tuning as an alternative and more accurate dating method than radiometric methods. By orbitally tuning two deep-sea cores (V28-238, V28-239) to eccentricity, he arrived at a date of 790 Kyr BP (thousand years before present) for the Brunhes-Matuyama magnetic reversal. This approach has recently been extended to cover the past 2.5 million years (e.g., Shackleton et al., 1990; Hilgen et al., 1993).

Imbrie et al. (1984) developed the orbitally tuned SPECMAP time scale from a stack of 5 tuned $\delta^{18}O$ records from deep-sea sediment cores. Three of the cores (V28-238, V22-174, DSDP502b) penetrate the Brunhes-Matuyama magnetic reversal, which Imbrie et al. dated from radiometric studies at 730 Kyr BP. Two of the cores (V30-40, RC11-120) are of higher resolution but shorter (~300 Kyr BP). Several radiometric control points were used in the first 100 Kyr BP. In the process of orbital tuning, Imbrie et al. included 56 to 72 control points and required approximately 120 iterations. Their target curves were obliquity and precession signals, phase-shifted by an ice-sheet model. The resulting SPECMAP curve shows high coherence in the correct orbital frequencies. Even though tuning was done only in the precession and obliquity bands, a strong peak containing a large part of the variance appeared near the 100 Kyr cycle, corresponding to a main eccentricity peak. Imbrie et al. (1984) concluded that as much as 85% of the isotopic variance in the orbital bands, or 60% of the *total* isotopic variance, may be explained by orbital forcing.

Martinson et al. (1987) used four different target curve versions in orbitally tuning a high resolution short core (RC11-120) and estimated that 25% of the complete $\delta^{18}O$ record could be explained as linear response to obliquity and precession; and if the ~100 Kyr component of eccentricity was included in the orbital forcing, the above value has risen from 25% to about 50%.

Can the eccentricity variations force a dominant 100 Kyr climate response? Eccentricity

can affect the incoming solar radiation only indirectly by modulating the amplitude of radiation changes caused by precessional variations. Various theories have been offered to explain how this eccentricity modulation can translate into a dominant eccentricity forcing, some of which are reviewed by Imbrie et al. (1993) and by Neeman et al. (1988a, 1988b). A common feature among these theories is that they were only tested with highly parameterized and tentative formulations relying heavily on tuning, thus successfully simulating a fair match with the SPEC-MAP record, though each had invoked different and unrelated mechanisms.

However, a more basic question is whether the precessional radiation variations, even when coupled with the obliquity radiation variations, are able to produce large climate changes. Neeman et al. (1988a) showed that testing the orbital theory with a climate model is closely linked with the broader and yet unresolved question of climate model sensitivity. Satisfactory reproduction of the present-day climate does not necessarily imply a model that has the correct climate sensitivity. The approach of Neeman et al. was to explore a range of variability of several tunable climate-model parameters, rather than to tune these parameters to a single optimal set of values.

Consequently, the current state of affairs is that climate models with realistic sensitivity do not simulate the initiation of ice-sheets even with extreme orbital parameters (Neeman et al., 1988b; Rind et al., 1989). In the former study, a statistical-dynamical zonally-sectorially averaged model was coupled to a vertically integrated ice sheet model with two horizontal dimensions. In the latter study, the GISS (Goddard Institute for Space Studies) GCM (general circulation model) was employed. Neeman et al. (1988b) demonstrated that whereas tuning the climate model to be more sensitive was a merit in simulating ice-sheet initiation, it turned out to be a stumbling block when the coupled model was designated to simulate a termination with a large ice sheet as initial condition. In response to a continuous application of extreme orbital parameters yielding highest summer insolation, most of the North American ice sheet has remained intact for the whole range of variability of climate-model and ice-sheet-model parameters. Similar results followed with a coupled ice-sheet - global seasonal energy balance model

with two horizontal dimensions developed by Deblonde and Peltier (1991). They stressed that the non-prediction of ice sheet collapse was robust against parameter variations in both parts of their coupled model.

If extreme values of precession and obliquity applied continuously cannot simulate either initiation or termination, then either all climate models are missing one or several important mechanisms, or the possibility exists that indeed modulating precession by eccentricity cannot create a dominant 100 Kyr ice-sheet variation. The latter conclusion is supported by Winograd et al. (1992) who investigated $\delta^{18}O$ variations in a continental core (DH-11) of vein calcite extending beyond 550 Kyr BP. Ages were assigned to the $\delta^{18}O$ data by interpolating between 21 mass-spectrometer uranium-series-dated intervals. They conclude that three out of four terminations recorded by the DH-11 record either preceded (II and III) or are not associated with (V) major insolation peaks, suggesting that terminations are not orbitally induced.

Recently, the possibility of a missing mechanism was brought up by Lindzen (personal communication, 1992) who suggests that small orbitally forced changes in the displacement of the solstitial surface temperature maximum (of the order of 2-3 degrees of latitude) produce large changes in the intensity of the Hadley circulation, which in turn are likely to play a significant role in determining the meridional heat fluxes in the winter hemisphere. A qualitative relation connecting intermediate and extreme heat fluxes to high and low snowfall respectively, results in the demodulation of the precession forcing leading to the dominant eccentricity periods.

The dominant 100 Kyr climate fluctuation, and its absence prior to 900 Kyr B.P. were simulated as a free oscillatory solution to a set of three low order equations relating ice, CO_2 and North Atlantic Deep Water formation (Saltzman and Sutera, 1987; Saltzman and Maasch, 1988; Maasch and Saltzman, 1990). Including non-eccentricity orbital forcing in the equation for rate of ice, an agreement of the ice solution with the SPECMAP $\delta^{18}O$ curve was achieved. The magnitude of the orbital forcing term was determined by an arbitrarily tuned constant.

It is worth emphasizing here the argument by Saltzman (1984), that whatever progress is made in climate modeling, the uncertainties of the physical parameterizations may always remain larger than the accuracy in snow budget calculations needed for prediction of the evolution of the ice sheets. A possible exception to this rule is a highly ablative negative snow budget that inhibits the formation of ice sheets, as found in the initiation experiment by Neeman et al. (1988b) and Rind et al. (1989).

In the present study, the orbital tuning approach is reassessed. Software is developed for real-time orbital tuning (Section 2) and applied to the analysis of the stacked $\delta^{18}O$ SPECMAP record (Section 3). One of the long range records composing the stack (V28-238) is analyzed before and after being orbitally tuned (Section 4). A random number series is taken as input curve (Section 5) and tuned to match the earth's orbital variations, followed by some experiments with the V28-238 record (Section 6) and a discussion (Section 7) of the orbital tuning approach and its significance in the evaluation of the role of orbital forcing.

2. The Software

A computer program was developed on an IBM-PC, with graphic and mathematical capabilities to perform a quick and real-time orbital tuning of any input record. The tuning is performed by clicking a control point on the graph of the input record and pulling it to the right or to the left along the time axis, by employing the keyboard cursors. After this is performed, the program calculates the new depth vs. time calibration function, which is a mapping function relating the untuned to the tuned curve, and from it evaluates the new tuned curve. Each shifted point has of course the same amplitude as before but it corresponds to a new time on the time axis. In addition, the program performs a quick spectral analysis of the resulting tuned curve, displaying a graph of the resulting spectrum compared with the orbital spectrum and displaying the coherence function (or squared coherence) between the tuned and orbital curves (see Diggle, 1990, Chapter 8). The whole process is instantaneous (on a 486/25-MHz PC with math co-processor), and the user sees the result immediately on the computer screen.

A menu-driven choice is available for comparing the input record which is being tuned to one (or more) of a set of curves. These include the eccentricity (e), the obliquity (ε) and the precession index ($e \sin\tilde{\omega}$, where $\tilde{\omega}$ is the longitude of perihelion), a combined orbital curve which is a normalized and phase-shifted combination of the above, and the original untuned curve. These curves appear with different colors to aid the tuning process. The orbital parameters as a function of time are calculated from tables and equations supplied by Berger (1978).

Filtered curves are obtained by summing the spectral components of the curve in only one of the orbital bands. At any point of the iteration the user can see the resulting filtered tuned curve as function of time, and compare it to the orbital curve in this band, checking visually for coherence, i.e., the extent to which wave patterns and envelopes are similar in the two curves (for the given frequency band). The program also accepts as input a given depth-in-core vs. time calibration function, either for an option of automatic tuning according to this input function, or for the sake of being displayed and compared with the calibration function arrived at during different steps in the orbital tuning. With the software developed in the present study, the whole process of orbital tuning is reduced to a matter of minutes.

3. The SPECMAP stack

As a first input to the program, the SPECMAP smoothed stack (Table 7, Imbrie et al., 1984) was taken. Here no tuning was done in the present study, since the SPECMAP curve (Fig. 1a, solid curve) is already tuned. The coherence function between the SPECMAP and orbital curves (Fig. 1b) shows peaks above 0.9 in or near all four orbital bands. Note that the scale of the coherence function is linearly compressed between 0 and 0.8 since peaks below 0.8 are in practice meaningless.

To be precise, the peaks are at 19-20, 22-25, 39-44 and 87 Kyr. The values of the peaks and their location on the period-frequency axis are in very good agreement with the coherency calculated by Imbrie et al. (1984) and shown in their Fig. 10. The shift of the 100 Kyr eccentricity peak to near 87 Kyr can also be seen there, only that it is less pronounced since

coherency is plotted in their case against frequency. (A plot against frequency has its advantages. However, for the ease of comparison with the orbital periods it was found more convenient to check against a linear period axis.) This shift of the coherence peak to 87 Kyr is an expression of the fact that if we combine the spectral components of the SPECMAP and orbital curves at the 87-112 Kyr band (Fig. 2c) and at the 78-98 Kyr band (Fig. 2d) and compare the results, a better match is seen in the latter band (compare the timing of the wave crests at 100 and 200 Kyr BP).

The match between the SPECMAP and orbital power spectrum (Fig. 1c) is even more striking here than in Fig. 10 of Imbrie et al. (1984), since the spectral analysis in the present study is of higher resolution and it captures the double peak near 23 Kyr (e.g., see Berger, 1977, Table 1) in both orbital and SPECMAP curves. Note that the dotted curve is a normalized and phase-shifted combination of e, ε and $e \sin\tilde{\omega}$. The phases of obliquity and precession in this combination were shifted, for the sake of comparison, to match the phases of the SPECMAP curve. The coefficients multiplying each orbital term in this combination were chosen in the present study to achieve agreement in amplitude with the SPECMAP curve in each of the three orbital bands. This agreement is of course artificial (intended for the sake of comparison), in contrast with agreement in the location of the peaks on the period axis and the fine structure in the 19-24 Kyr band of the precession index, that is indeed striking. As a matter of fact, Imbrie et al. argued that it would be difficult to see how coherencies ranging from 0.92 to 0.97 could be achieved in all four frequency bands simultaneously as an artifact of the tuning procedure (however, see below).

A word of caution, though, regarding the coherence in the eccentricity band. The fact that the peak in coherence function is shifted was already discussed above. What is even more meaningful is the absence of any significant coherencies at or near the other spectral peaks of eccentricity, like 120 and 400 Kyr, see Fig. 2a,b. Thus, if the spectral components of the SPECMAP and orbital curves are compared in the 49-392 Kyr band, Fig. 1d, similarity is poor, in contrast with the remarkable match in the precession band in Fig. 1f. The latter

coherence was of course one of the main findings of Imbrie et al. (1984) in their Fig. 9, and agreement between the latter figure and Fig. 1 serves as a verification for the results of the present study.

The spectrum of significant coherencies (>0.75) and their phases are given in Table 1. A generally small range of phases indicates (or results from) an agreement with the target (phase-shifted) orbital curve, though deviations from -20 to +30 degrees exist. In particular, there is a deviation between 19 and 21 Kyr that cannot be explained by the theoretical phase curve of Imbrie et al. (1984) (see their Fig. 11).

4. The V28-238 record

The untuned raw $\delta^{18}O$ record from the V28-238 core (Shackleton and Opdyke, 1973; Pisias, personal communication, 1992) was used as input to the program. Actually, Imbrie et al. (1984) modified the raw record by removing a 30-cm section (723-753 cm) which they represent as stretching of the record during core recovery, and this was also repeated for consistency in the present study. A constant sedimentation rate was assumed by assigning the date of 731 Kyr BP to depth 1171 cm (the SPECMAP timing of the Brunhes-Matuyama magnetic reversal, Table 6, Imbrie et al., 1984). The modified untuned V28-238 record is shown in Fig. 3, compared with the orbital combination (dotted curve) having the same parameters as for the SPECMAP case discussed above. The power spectrum (Fig. 3c) shows a rather continuous spectrum, with a peak at 43.6 Kyr which may be related to the nearby obliquity peak, and also a small peak at 19.1 Kyr with high coherence with the orbital signal. Apart from the latter, there is no significant coherence, and there is no reason to expect for one since the record is untuned and sedimentation rates may change in time. The aforementioned coherence peak, as well as a peak near 60 Kyr may well be coincidental peaks, as judged from experience with various records analyzed in the present study.

Next, the calibration function for the SPECMAP tuning of V28-238 was taken as input to the program from Table 6 of Imbrie et al. (1984). Using the automatic tuning option, the

record was tuned and analyzed in Fig. 4. Compare the tuned and untuned (Fig. 3) records and observe the shrinking and stretching of various sections along the time axis. There is a high resemblance between the coherence and power spectrum of the individual V28-238 tuned record and that of the stack shown in Fig. 1. Again the coherence is above 0.9 in the precession and obliquity bands and in 87 Kyr, and the fine structure of the power spectrum agrees with that of the orbital signal. Resemblance between the two experiments is also found in the individual bands. A remarkable match is again seen in the precession band (Fig. 4f). In contrast, there is no coherence in any band in the untuned V28-238 record (Fig. 3).

5. A Random Record

Fig. 5 shows a random series record. Here a series of 392 numbers was taken by calling the random function of the Turbo-C Borland Library. Prior to using the random function, it must be "seeded" with an integer, chosen here as 13, hence the name RANDOM 13. Each random number was assigned a date starting with 0 Kyr BP with a time interval of 2 Kyr. As the original series showed too much fluctuation at high frequencies, it was passed through a low-pass filter shown in Fig. 6. The resulting series was scaled to units of standard deviation and plotted in Fig. 5 on the $\delta^{18}O$ axis. The dotted curve is again the same orbital combination used above in the SPECMAP stack comparison.

There is no significant coherence with the orbital signal (Fig. 5b) except for a coincidental peak of 0.84 at 28 Kyr. The power spectrum is rather continuous with some peaks, e.g. near 50 Kyr, showing some resemblance in nature to the power spectrum of the untuned V28-238 (compare Fig. 5c, with Fig. 3c). The decomposition of the untuned RANDOM 13 record into the three orbital bands (Fig. 5d,e,f) shows little similarity (coherence) with the orbital signal, in resemblance to the untuned V28-238 case (Fig. 3d,e,f).

In Fig. 5a each cross represents a control point which was allowed to be tuned in the tuning procedure. The distance between the control points was initially fixed at 12 Kyr, and there were 65 such control points. This is a rather more strict condition placed on the current tuning

procedure compared to the one employed in the SPECMAP tuning, where control points were added wherever needed (56-72 for the different cores).

In the process of tuning, the RANDOM 13 curve was mainly tuned against the orbital combination curve obtained for the SPECMAP case and described above. Occasionally, the tuning was performed iteratively against the individual precession, obliquity and eccentricity curves in turn. This iterative procedure follows Imbrie et al. (1984), except that the present tuning was not designed to exclude eccentricity as a target curve (however, see below). At the later stages of the tuning, special attention was paid to changes in the coherence function, seen in real-time after each tuning step. Should the coherence decrease, the tuning would be reversed, i.e, the control point returned to its previous position along the time axis.

The resulting tuned RANDOM 13 curve is shown in Fig. 7. A striking agreement was obtained in the power spectrum (Fig. 7c) in the obliquity and precession bands, including the fine detail in the 19.1, 22.4 and 23.8 Kyr peaks. Coherence (Fig. 7b) throughout these bands is above 0.95 and is above 0.90 in a single peak in the eccentricity band (112 Kyr). The peak in the power spectrum (Fig. 7c) in 100 Kyr is smaller in amplitude than the orbital combination (dotted) curve, a fact that has little meaning remembering that the coefficient of eccentricity in orbital combination curve was chosen in the present study (see above) so that the amplitude of the power spectrum at 100 Kyr agree with the SPECMAP tuned peak. Note also that near 100 Kyr, the untuned RANDOM 13 curve (Fig. 5c) has less power than the untuned V28-238 curve (Fig. 3c).

The tuned RANDOM 13 curve, filtered to include only components in the precession band (Fig. 7f) shows a remarkable match with the orbital precession curve (dotted curve), to no lesser extent than the filtered SPECMAP curve (Fig. 1f) or the filtered tuned V28-238 curve (Fig. 4f). Evidently, this remarkable match is not more than an agreement in amplitude and phase between each of the spectral components of the tuned and target curves, and the present tuning experiment proves that tuning may achieve agreement for various wave components

simultaneously. Once the wave components of the tuned and target curves agree in a particular band, the filtered tuned and target curves will also agree in that band.

Table 2 shows the spectrum of significant coherencies (>0.75) and their phases. The range of phases is even smaller than for the SPECMAP curve (Table 1) indicating (or resulting from) a match between the tuned and target curves.

The calibration curve for the tuned RANDOM 13 curve is presented in Fig. 8a (solid line) and compared with the calibration curve of the SPECMAP tuned DSDP502b core (dotted line) obtained from Table 6 of Imbrie et al. (1984) (see their Fig. 7 for the calibration curves for all 5 cores). The slope (or sedimentation rate) of the RANDOM 13 calibration curve lies within the range of the slopes of the SPECMAP calibration curves, as demonstrated in Fig. 8b.

Following a reviewer's request, two additional tuning experiments were conducted on RANDOM 13, both *excluding* eccentricity from the target orbital curve. Results are shown in Figs. 9 and 10. The target curve used in the process of tuning is the dotted curve in Figs. 9a and 10a. Calculations of coherence and power spectrum are performed with the complete phase-shifted orbital combination curve. In one experiment (Fig. 9), in the process of maximizing the coherence in the obliquity and precession bands, a 100 Kyr peak has spontaneously appeared. In the other experiment (Fig. 10) this phenomenon has not occurred. Note that the resulting power spectrum (Figs. 9c and 10c) at 100 Kyr is considerably lower than in the original tuning experiment (Fig. 7c) where eccentricity was included in the target curve. A corollary is the non-uniqueness of the tuning solution.

It was verified that the results with the RANDOM 13 curve are not dependent upon the choice of 13 as a seed. All other seeds tested have produced random curves which could be orbitally tuned to the same extent as RANDOM 13, i.e., resulting in each case in matching spectral power peaks with coherencies above 0.95 in the three bands corresponding to precession and obliquity, and above 0.9 near the 100 Kyr eccentricity cycle.

6. The Portion of Orbital Forcing in Untuned Records

What is the portion of the variance in the deep-sea core records that can be attributed to the orbital forcing? The results of the present study rule out such an estimate based on orbital tuning. Returning to the untuned (modified, see above) V28-238 curve, Fig. 3, the peaks in the power spectrum near 19, 22 and 43.5 Kyr were "smoothed out" by reducing the amplitude of these wave components manually to a mean amplitude of neighboring waves, and subsequently rebuilding the curve from its modified wave components. The resulting curve, shown in Fig. 11a, is not very different from the original, Fig. 3a, except for the absence of some very small fluctuations, and the corresponding smoother power spectrum (Fig. 11c). Similar results (not shown here) follow with the two other SPECMAP stack deep-sea sediment cores, V22-174 and DSDP502b, also covering the entire Brunhes Epoch. An assumption of constant sedimentation rate therefore leads to a negligible orbital trace in the $\delta^{18}O$ signal of deep-sea core records.

In the original constant sedimentation time scale of Shackleton and Opdyke (1973), the Brunhes-Matuyama reversal is dated 700 Kyr BP. Using this date instead of 731, the results shown in Fig. 12 were obtained. Here the peaks near 19, 22 and 43.5 Kyr are shifted to 18, 21 and 41 Kyr respectively, while their amplitude remain about the same. New small peaks appear near 23 Kyr. Comparison with the orbital power spectrum (dotted line) is now better for obliquity and worse for precession. However, there is no coherence in any orbital band (Fig. 12b).

However, the assumption of constant sedimentation rate may be too rigid since this rate is known to vary in time. What may be suitable is therefore an independent time scale, with the precision of mass-spectrometric dating and not making any use of orbital tuning. Fortunately, such time scale exists, though it has not received much attention, and it was developed for none other than the V28-238 core. Kominz et al. (1979) measured aluminum and other major element concentrations at short intervals down this core by flame atomic absorption spectro-

photometry. The aluminum content of sampled intervals was found from its concentration, the length of the interval and the bulk density calculated from chloridometer measurements. The sampled intervals were taken as the $\delta^{18}O$ stages (Shackleton and Opdyke, 1973, see also below). For the first 10 stage boundaries (first 362 Kyr), dating was determined from ^{230}Th activities. Kominz et al. demonstrated that dating by the assumption of constant aluminum accumulation rate highly correlated with the independent ^{230}Th dating.

It is not implied here that the aluminum scale is necessarily better than other time scales. Absolute time calibration of paleoclimatic records is most likely still inaccurate and the aluminum scale may be outdated. With this reservation in mind, the aluminum scale of Kominz et al. is tested in the present study, using their Table 4 as calibration. Each of the first 19 control points is a stage boundary, shown as a cross in Fig. 13a. The 20th (oldest) control point is the Brunhes-Matuyama boundary given as 693 Kyr BP. Note that the boundary between stage 5 and 6 (Termination II) is given as 138 Kyr BP by the aluminum scale, and was considered too old in 1979. However, today it is the main focus of attention, dated as 140 Kyr BP in the Devils Hole DH-11 record (Winograd et al., 1992) and in the original Vostok record chronology (Jouzel et al., 1987), and also in the Summit record (Dansgaard et al., 1993), but dated as 128 Kyr BP in the SPECMAP record (Imbrie et al., 1984).

Comparing the analysis of the aluminum scale (Fig. 13) with that of the constant sedimentation scales (Figs. 3 and 12), there is no evidence that a similarity with the orbital signal has improved. On the contrary, the power spectrum is smoother with the aluminum scale, without peaks that can be related to orbital periods, and coherence in the orbital bands is low. Very similar results (not shown here) were obtained by replacing the first 10 aluminum dates by the corresponding ^{230}Th dates. Comparison of the calibration function of the aluminum scale with that of the SPECMAP scale (Fig. 14a) shows that it is smoother for the aluminum scale, with sedimentation rates (Fig. 14b, solid line) varying considerably less than for the SPECMAP scale (Fig. 14b, dotted line).

7. Discussion

The random curve experiment performed in the present study clearly demonstrates that coherencies above 0.9 in the precessional and obliquity orbital bands and near the 100 Kyr eccentricity period may be achieved simultaneously as an artifact of orbital tuning. The original untuned random curve has of course no coherence with the orbital signal, and the tuning performed is within the range of constrictions common in other marine chronostratigraphic studies. The risks of orbital tuning were already recognized (e.g., Pestiaux and Berger, 1984; Pisias and Leinen, 1984). The former argued that the weaker the tuning assumptions will be, the larger are the chances to avoid circularity; while the latter suggested that the presence of a spectral peak lying close to an orbital frequency may not be related to orbital forcing at that frequency. However, Pisias (1983) indicated the inability to produce either an increase in coherence or to induce the presence of spectral peaks by "orbitally tuning" a random number series. Recently, using a similar strategy, Brüggemann (1992) noted that coherence could be increased, but only in one frequency band at a time.

The results of the present random curve experiment and the extent to which it was successful in reproducing a high match with the orbital signal leaves little doubt as to the ability of orbital tuning to introduce artificial power in the spectra of the original records. Evidently, orbital tuning cannot be the basis of any support for the orbital theory, nor can it be used for quantitative estimates of the portion of orbital forcing.

Recognizing the potential circularity of orbital tuning, Imbrie et al. (1984) relied in their conclusions on the fact that they performed their orbital tuning only in the precession and obliquity bands, while obtaining a significant coherence peak in the eccentricity band. Tuning a random curve in the present study to a target curve comprising of only precession and obliquity signals has resulted in one instance in the appearance of a coherence peak at 100 Kyr. In the experiment where eccentricity was *included* in the target curve, the power of the tuned curve at 100 Kyr was higher, and overall resemblance was best.

Therefore, the phenomenon observed by Imbrie et al. should not be regarded as a proof of the orbital theory, though it may be connected to this theory by an explanation offered by Neeman et al. (1988a). The connection is through the well known fact that precession is modulated by eccentricity (the envelope of the precession signal is proportional to the eccentricity signal, see for example Fig. 1f, dotted line). Therefore it is possible that by aligning the long-scale fluctuations to form a 100 Kyr sinus wave, it is then easier to obtain a 100 Kyr modulation of the near 20 Kyr small-scale fluctuations. The fact that the spectral power in 100 Kyr has increased is essentially a result of this alignment, which in turn is equivalent to tuning to 100 Kyr. Therefore, the phenomenon observed by Imbrie et al. can be restated as follows: tuning to 100 Kyr in addition to tuning to obliquity and precession results in better coherencies in all orbital bands.

It may be difficult to see in the orbitally tuned SPECMAP curve a proof that eccentricity variations are linked with climate, since coherence with the eccentricity peak is limited to a narrow peak at 87 Kyr, while the eccentricity spectral power at 120 and 400 Kyr is completely absent in the tuned curve. As mentioned in Section 1, there are a few theories which might explain non-linear climate forcing by the eccentricity signal. However, it would not be straightforward to explain a dominant climatic peak at 100 Kyr, while also providing an explanation for the absence of the 120 and 400 Kyr peaks, or even the absence of the main 100 Kyr peak prior to 900 Kyr BP (e.g., Pisias and Moore, 1981).

The untuned long-range $\delta^{18}O$ records composing the SPECMAP stack do not exhibit spectral power peaks at the eccentricity periods. On the other hand, they do show some relatively small peaks near obliquity and precession periods. These peaks may be close to orbital periods by mere coincidence. Many random curves that were tested in the present study had power spectra of the same nature with peaks of similar relative magnitude at or near orbital periods, even before tuning. Alternatively, if they do represent the blurred contribution of orbital forcing, the experiment of smoothing out the peaks has illustrated that this contribution is negligible. Analyzing the V28-238 $\delta^{18}O$ record with the independent aluminum time scale

of Kominz et al. (1979), anchored by 11 ^{230}Th dates, shows even less similarity with the orbital signal, emphasizing that a match with the orbital signal was obtained only after performing orbital tuning.

The results of the present study seriously question the practice of dating geological events from orbitally tuned time scales. This conclusion is self-evident if most of the power in paleoclimatic records is of non-orbital origin. But even if it turns out that orbital variations do leave a significant trace in the records, orbital tuning is not the right tool to recover it. The sedimentation rate of untuned records varies and they are disturbed by a list of factors mentioned in Section 1, and the power spectrum of untuned records is undoubtedly very noisy. Consequently, it follows that the solution of orbital tuning is non-unique.

Acknowledgments

The author is grateful for the prompt help of N. Pisias in providing datasets of deep-sea records and detailed answers. Discussions with R. Lindzen and his encouragement are appreciated. The author acknowledges the constructive comments made by the Journal of Climate reviewers.

REFERENCES

Berger, A. L., 1977: Support for the astronomical theory of climate change. *Nature*, **269**, 44-45.

Berger, A. L., 1978: Long term variations of daily insolation and quaternary climatic changes. *J. Atmos. Sci.*, **35**, 2363-2367.

Brüggemann, W., 1992: A minimal cost function method for optimizing the age-depth relation of deep sea sediment cores. *Paleoceanography*, **7**, 467-487.

Dansgaard, W., S. J. Johnsen, H. B. Clausen, D. Dahl-Jensen, N. S. Gundestrup, C. U. Hammer, C. S. Hvidberg, J. P. Steffensen, A. E. Sveinbjörnsdottir, J. Jouzel and G. Bond, 1993: Evidence for general instability of past climate from a 250-kyr ice-core record.

Nature, **364**, 218-220.

Deblonde, G. and W. R. Peltier, 1991: Simulations of continental ice sheet growth over the last glacial-interglacial cycle: Experiments with a one-level seasonal energy balance model including realistic geography. *J. Geophys. Res.*, **96**, 9189-9215.

Diggle P. J., 1990: *Time Series: A Biostatistical Introduction*, 257pp, Oxford University Press, Oxford.

Evans, D. L., and H. J. Freeland, 1977: Variations in the Earth's orbit: pacemaker of the ice ages? *Science*, **198**, 528-530.

Hays, J. D., J. Imbrie and N. J. Shackleton, 1976: Variations in the Earth's orbit: pacemaker of the ice ages. *Science*, **194**, 1121-1132.

Hilgen, F. J., L. J. Lourens, A. Berger and M. F. Loutre, 1993: Evaluation of the astronomically calibrated time scale for the late Pliocene and earliest Pleistocene. *Paleoceanography*, **8**, 549-565.

Imbrie, J., J. D. Hays, D. G. Martinson, A. McIntyre, A. C. Mix, J. J. Moreley, N. G. Pisias, W. L. Prell and N. J. Shackleton, 1984: The orbital theory of Pleistocene climate: Support from a revised chronology of the marine $\delta^{18}O$ record. *Milankovitch and Climate*, A. Berger, J. Imbrie, J. Hays, G. Kukla and B. Saltzman, Eds., D. Reidel, 269-306.

Imbrie, J., A. Berger, E. A. Boyle, S. C. Clemens, A. Duffy, W. R. Howard,G. Kukla, J. Kutzbach, D. G. Martinson, A. McIntyre, A. C. Mix, B. Molfino, J. J. Morley, L. C. Peterson, N. G. Pisias, W. L. Prell, M. E. Raymo, N. J. Shackleton and J. R. Toggweiler, 1993: On the structure and origin of major glaciation cycles. 2. The 100,000-year cycle. *Paleoceanography*, **8**, 699-735.

Johnson, R. G., 1982: Brunhes-Matuyama magnetic reversal dated at 790,000 yr B.P. by marine-astronomical correlations. *Quat. Res.*, **17**, 135-147.

Jouzel, J., C. Lorius, J. R. Petit, C. Genthon, N. I. Barkov, V. M. Kotlyakov and V. M. Petrov, 1987: Vostok ice core: a continuous isotope temperature record over the last

climatic cycle (160,000 years). *Nature*, **329**, 403-408.

Kominz, M. A., G. R. Heath, T.-L. Ku and N. G. Pisias, 1979: Brunhes time scales and the interpretation of climate change. *Earth Planet. Sci. Lett.*, **45**, 394-410.

Maasch, K. A., and B. Saltzman, 1990: A low-order dynamical model of global climatic variability over the full Pelistocene. *J. Geophys. Res.*, **95**, 1955-1963.

Martinson, D. G., W. Menke and A. Stoffa, 1982: An inverse approach to signal correlation. *J. Geophys. Res.*, **87**, 4807-4818.

Martinson, D. G., N. G. Pisias, J. D. Hays, J. Imbrie, T. C. Moore, Jr., and N. J. Shackleton, 1987: Age dating and the orbital theory of the ice-ages: Development of a high-resolution 0 to 300,000-year chronostratigraphy. *Quat. Res.*, **27**, 1-29.

Milankovitch, M., 1941: Canon of insolation and the ice age problem. *K. Serb. Acad. Beogr. Spec.*, Publ. 132, Translated by the Israel Program for Scientific Translations, Jerusalem, 1969, 482 pp.

Neeman, B. U., G. Ohring and J. H. Joseph, 1988a: The Milankovitch theory and climate sensitivity: 1. Equilibrium climate model solutions for the present surface conditions. *J. Geophys. Res.*, **93**, 11153-11174.

Neeman, B. U., G. Ohring and J. H. Joseph, 1988b: The Milankovitch theory and climate sensitivity: 2. Interaction between the northern hemisphere ice sheets and the climate system. *J. Geophys. Res.*, **93**, 11175-11191.

Pestiaux, P., and A. Berger, 1984: Impacts of deep-sea processes on paleoclimatic spectra. *Milankovitch and Climate*, A. Berger, J. Imbrie, J. Hays, G. Kukla and B. Saltzman, Eds., D. Reidel, 493-510.

Pisias, N. G. and M. Leinen, 1984: Milankovitch forcing of the oceanic system: evidence from the northwest Pacific. *Milankovitch and Climate*, A. Berger, J. Imbrie, J. Hays, G. Kukla and B. Saltzman, Eds., D. Reidel, 307-330.

Pisias, N. G. and T. C. Moore, Jr., 1981: The evolution of the Pleistocene climate: A time series approach. *Earth Planet. Sci. Lett.*, **52**, 450-458.

Pisias, N. G., 1983: Geologic time series from deep-sea sediments: time scales and distortion by bioturbation. *Mar. Geol.*, **51**, 99-113.

Rind, D., D. Peteet and G. Kukla, 1989: Can Milankovitch orbital variations initiate the growth of ice sheets in a general circulation model? *J. Geophys. Res.*, **94**, 12851-12871.

Saltzman, B., 1984: On the role of equilibrium atmospheric climate models in the theory of long-period glacial variations. *J. Atmos. Sci.*, **41**, 2263-2266.

Saltzman, B., and K. A. Maasch, 1988: Carbon cycle instability as a cause of the late Pleistocene ice age oscillations: Modeling the asymmetric response. *Global Biogeochem. Cycles*, **2**, 177-185.

Saltzman, B., and A. Sutera, 1987: The mid-Quaternary climatic transition as a free response of a three-variable dynamical model. *J. Atmos. Sci.*, **44**, 236-241.

Shackleton, N. J., A. Berger and W. R. Peltier, 1990: An alternative astronomical calibration of the lower Pleistocene timescale based on ODP Site 677. *Trans. R. Soc. Edinburgh Earth Sci.*, **81**, 251-261.

Shackleton, N. J. and N. D. Opdyke, 1973: Oxygen isotope and paleomagnetic stratigraphy of equatorial Pacific core V28-238: oxygen isotope temperature and ice volume on 10^5 year and 10^6 year scale. *Quat. Res.* **3**, 39-55.

Winograd, I. J., T. B. Coplen, J. M. Landwehr, A. C. Riggs, K. R. Ludwig, B. J. Szabo, P. T. Kolesar, K. M. Revesz, 1992: Continuous 500,000-year climate record from vein calcite in Devils Hole, Nevada. *Science*, **258**, 255-260.

Figure Legends

1. The SPECMAP stack of 5 orbitally tuned $\delta^{18}O$ records: (a) the SPECMAP curve (solid line) in standard deviation units plotted against time before present and compared with a

phase-shifted orbital combination curve (dotted line, see text), (b) the coherence function between the SPECMAP and the orbital curve (with linear compressed scale between 0 and 0.8) plotted against the period, (c) the power spectrum of the SPECMAP curve (solid line) and of the orbital combination curve (dotted line) plotted against period; (d) The SPECMAP curve (solid line) compared with the orbital combination curve (dotted line) filtered to include only components in the eccentricity band, (e) obliquity band, and (f) precession band, plotted against time before present.

2. (a) As in Fig. 1b and (b) as in Fig1c, but with scale of period axis extending to 400 Kyr; (c) The SPECMAP curve (solid line) compared with the orbital combination curve (dotted line) filtered to include only components in the 87-112 Kyr band and (d) in the 78-98 Kyr band, plotted against time before present.

3. As in Fig. 1 but for the V28-238 untuned $\delta^{18}O$ record.

4. As in Fig. 1 but for the V28-238 orbitally tuned $\delta^{18}O$ record.

5. As in Fig. 1 but for the RANDOM 13 untuned record.

6. The low-pass filter multiplying each wave component of the original RANDOM 13 curve.

7. As in Fig. 1 but for the RANDOM 13 orbitally tuned record.

8. (a) The calibration function for the RANDOM 13 orbitally tuned record (solid line) scaled to fit on top of the calibration function, depth vs. time, for the orbitally tuned DSDP502b $\delta^{18}O$ record (Table 6 of Imbrie et al., 1984), and (b) the sedimentation rate (or slope of the calibration function) for the RANDOM 13 (solid line) and the DSDP502b $\delta^{18}O$ record.

9. As in Fig. 7 but for a second experiment, in which the RANDOM 13 curve is orbitally tuned to a target curve comprising of only precession and obliquity signals (the dotted curve in (a)).

10. As in Fig. 9 but for an additional experiment, in which coherence did not increase near the 100 Kyr period.

11. As in Fig. 1a,b and c, but for the V28-238 untuned $\delta^{18}O$ record for which the wave components responsible for peaks near orbital frequencies were reduced to amplitudes of neighboring wave components, and the record rebuilt from its modified wave components.

12. As in Fig. 1a,b and c, but for the V28-238 untuned $\delta^{18}O$ record for which the Brunhes-Matuyama boundary was dated 700 Kyr BP (following the original Shackleton and Opdyke, 1973, time scale) instead of 731 Kyr BP (following the SPECMAP time scale).

13. As in Fig. 1a,b and c, but for the V28-238 $\delta^{18}O$ record calibrated by the independent constant aluminum accumulation time scale of Kominz et al. (1979), anchored by 11 ^{230}Th dates.

14. (a) The calibration function, depth vs. time, for the aluminum scale (solid line, Table 4 of Kominz et al., 1979) and the orbitally tuned SPECMAP scale (dotted line, Table 6 of Imbrie et al., 1984), both scales developed for the V28-238 $\delta^{18}O$ record, and (b) The sedimentation rate (or slope of the calibration function) for the aluminum scale (solid line) and the orbitally tuned SPECMAP scale (dotted line).

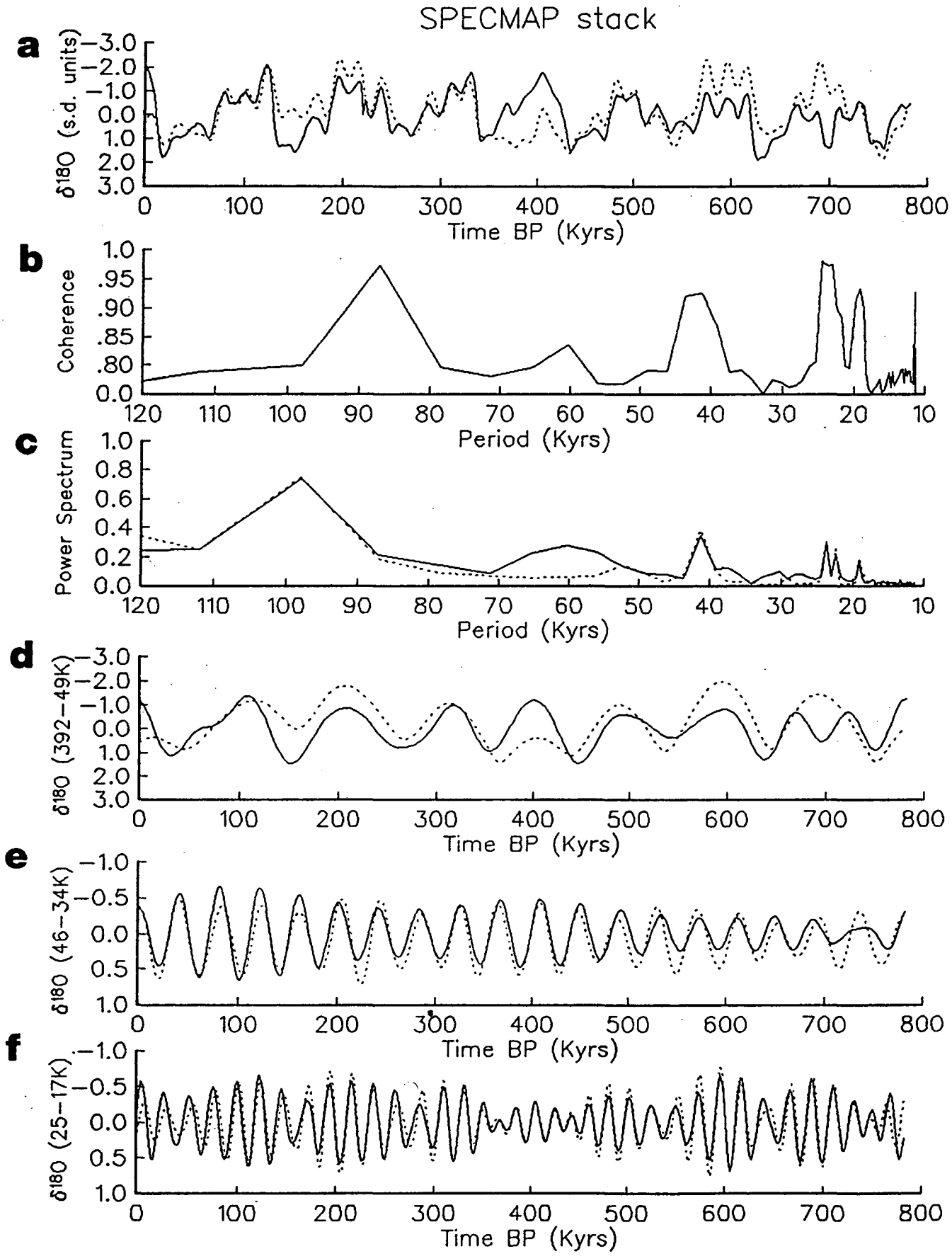
SPECMAP stack
a
δ18O (s.d. units)
−3.0
−2.0
−1.0
0.0
1.0
2.0
3.0
0
100
200
300
400
500
600
700
800
Time BP (Kyrs)
b
Coherence
1.0
.95
.90
.85
.80
0.0
120
110
100
90
80
70
60
50
40
30
20
10
Period (Kyrs)
c
Power Spectrum
1.0
0.8
0.6
0.4
0.2
0.0
120
110
100
90
80
70
60
50
40
30
20
10
Period (Kyrs)
d
δ18O (392−49K)
−3.0
−2.0
−1.0
0.0
1.0
2.0
3.0
0
100
200
300
400
500
600
700
800
Time BP (Kyrs)
e
δ18O (46−34K)
−1.0
−0.5
0.0
0.5
1.0
0
100
200
300
400
500
600
700
800
Time BP (Kyrs)
f
δ18O (25−17K)
−1.0
−0.5
0.0
0.5
1.0
0
100
200
300
400
500
600
700
800
Time BP (Kyrs)

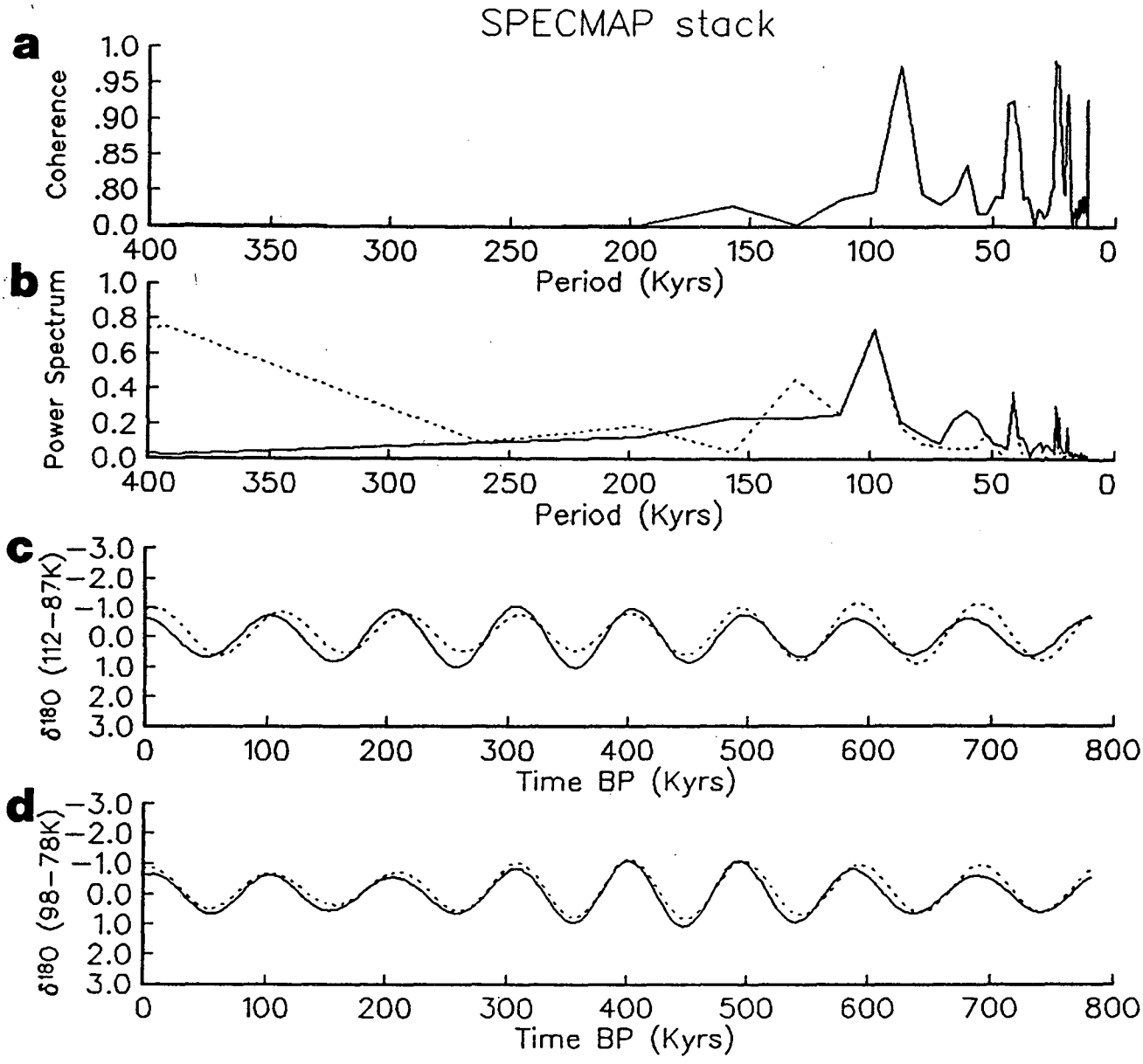
SPECMAP stack
a
Coherence
1.0
.95
.90
.85
.80
0.0
400
350
300
250
200
150
100
50
0
Period (Kyrs)
b
Power Spectrum
1.0
0.8
0.6
0.4
0.2
0.0
400
350
300
250
200
150
100
50
0
Period (Kyrs)
c
δ18O (112–87K)
−3.0
−2.0
−1.0
0.0
1.0
2.0
3.0
0
100
200
300
400
500
600
700
800
Time BP (Kyrs)
d
δ18O (98–78K)
−3.0
−2.0
−1.0
0.0
1.0
2.0
3.0
0
100
200
300
400
500
600
700
800
Time BP (Kyrs)

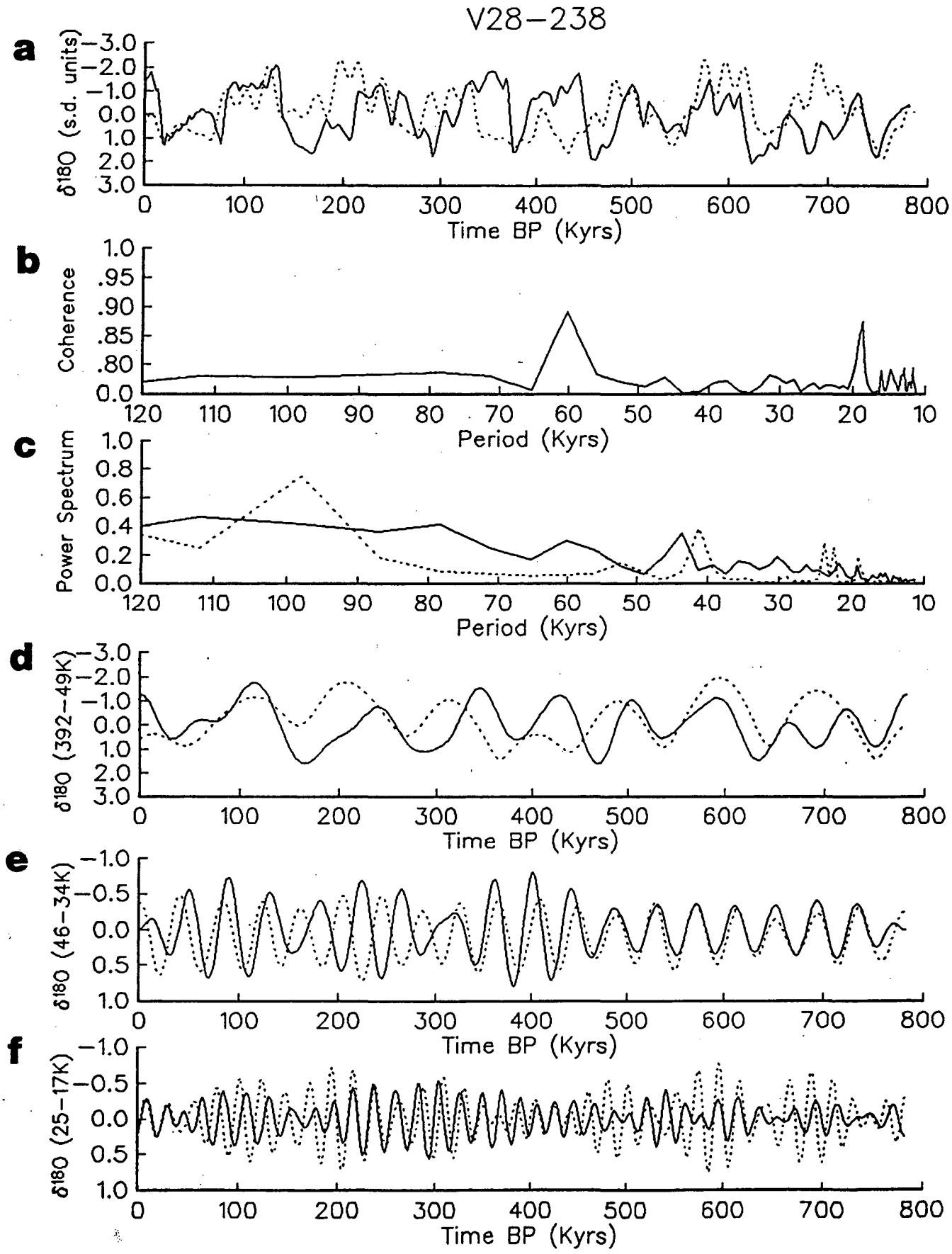
V28−238
a
δ18O (s.d. units)
−3.0
−2.0
−1.0
0.0
1.0
2.0
3.0
0
100
200
300
400
500
600
700
800
Time BP (Kyrs)
b
Coherence
1.0
.95
.90
.85
.80
0.0
120
110
100
90
80
70
60
50
40
30
20
10
Period (Kyrs)
c
Power Spectrum
1.0
0.8
0.6
0.4
0.2
0.0
120
110
100
90
80
70
60
50
40
30
20
10
Period (Kyrs)
d
δ18O (392−49K)
−3.0
−2.0
−1.0
0.0
1.0
2.0
3.0
0
100
200
300
400
500
600
700
800
Time BP (Kyrs)
e
δ18O (46−34K)
−1.0
−0.5
0.0
0.5
1.0
0
100
200
300
400
500
600
700
800
Time BP (Kyrs)
f
δ18O (25−17K)
−1.0
−0.5
0.0
0.5
1.0
0
100
200
300
400
500
600
700
800
Time BP (Kyrs)

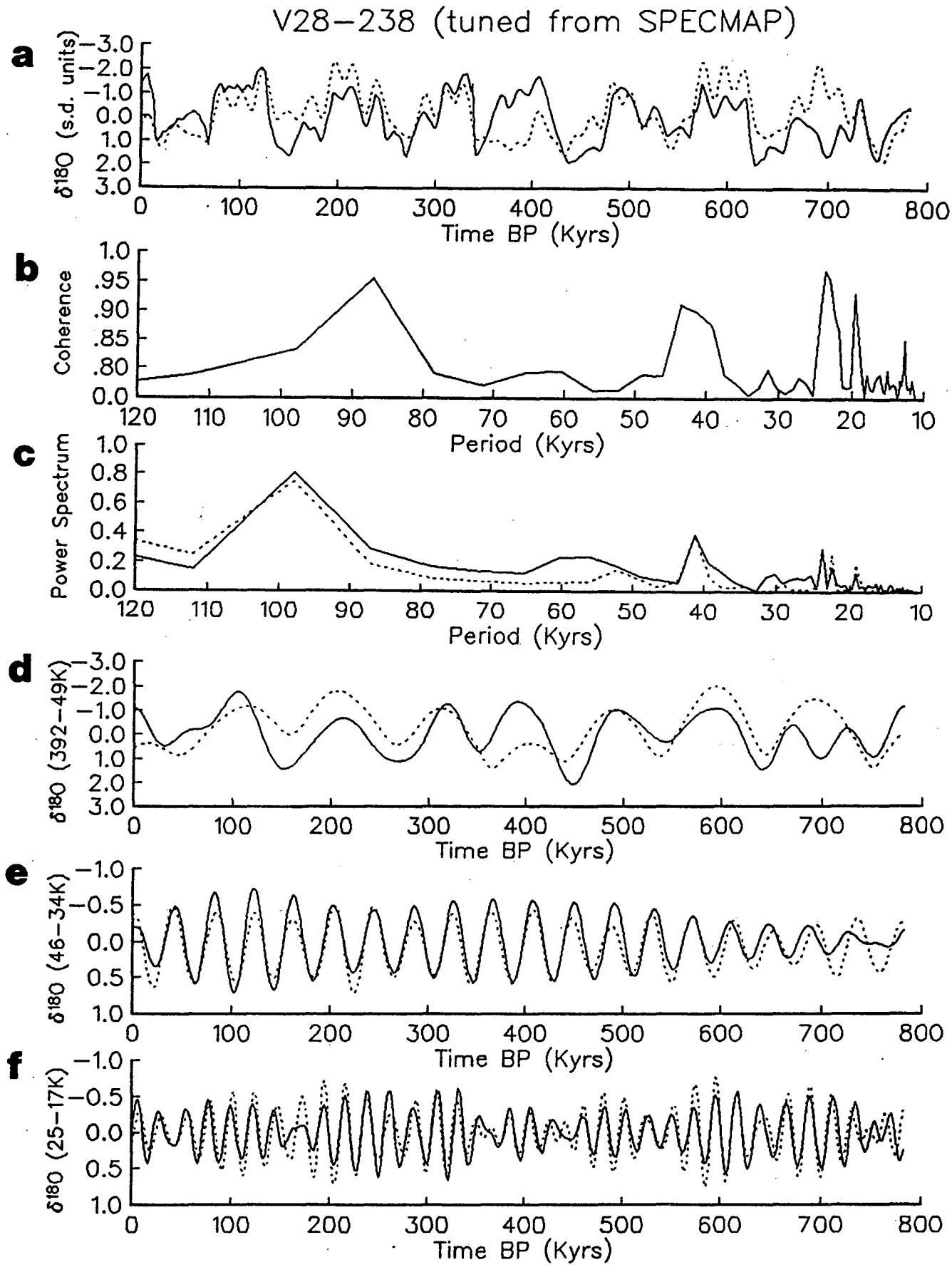
V28−238 (tuned from SPECMAP)
a
δ18O (s.d. units)
−3.0
−2.0
−1.0
0.0
1.0
2.0
3.0
0
100
200
300
400
500
600
700
800
Time BP (Kyrs)
b
Coherence
1.0
.95
.90
.85
.80
0.0
120
110
100
90
80
70
60
50
40
30
20
10
Period (Kyrs)
c
Power Spectrum
1.0
0.8
0.6
0.4
0.2
0.0
120
110
100
90
80
70
60
50
40
30
20
10
Period (Kyrs)
d
δ18O (392−49K)
−3.0
−2.0
−1.0
0.0
1.0
2.0
3.0
0
100
200
300
400
500
600
700
800
Time BP (Kyrs)
e
δ18O (46−34K)
−1.0
−0.5
0.0
0.5
1.0
0
100
200
300
400
500
600
700
800
Time BP (Kyrs)
f
δ18O (25−17K)
−1.0
−0.5
0.0
0.5
1.0
0
100
200
300
400
500
600
700
800
Time BP (Kyrs)

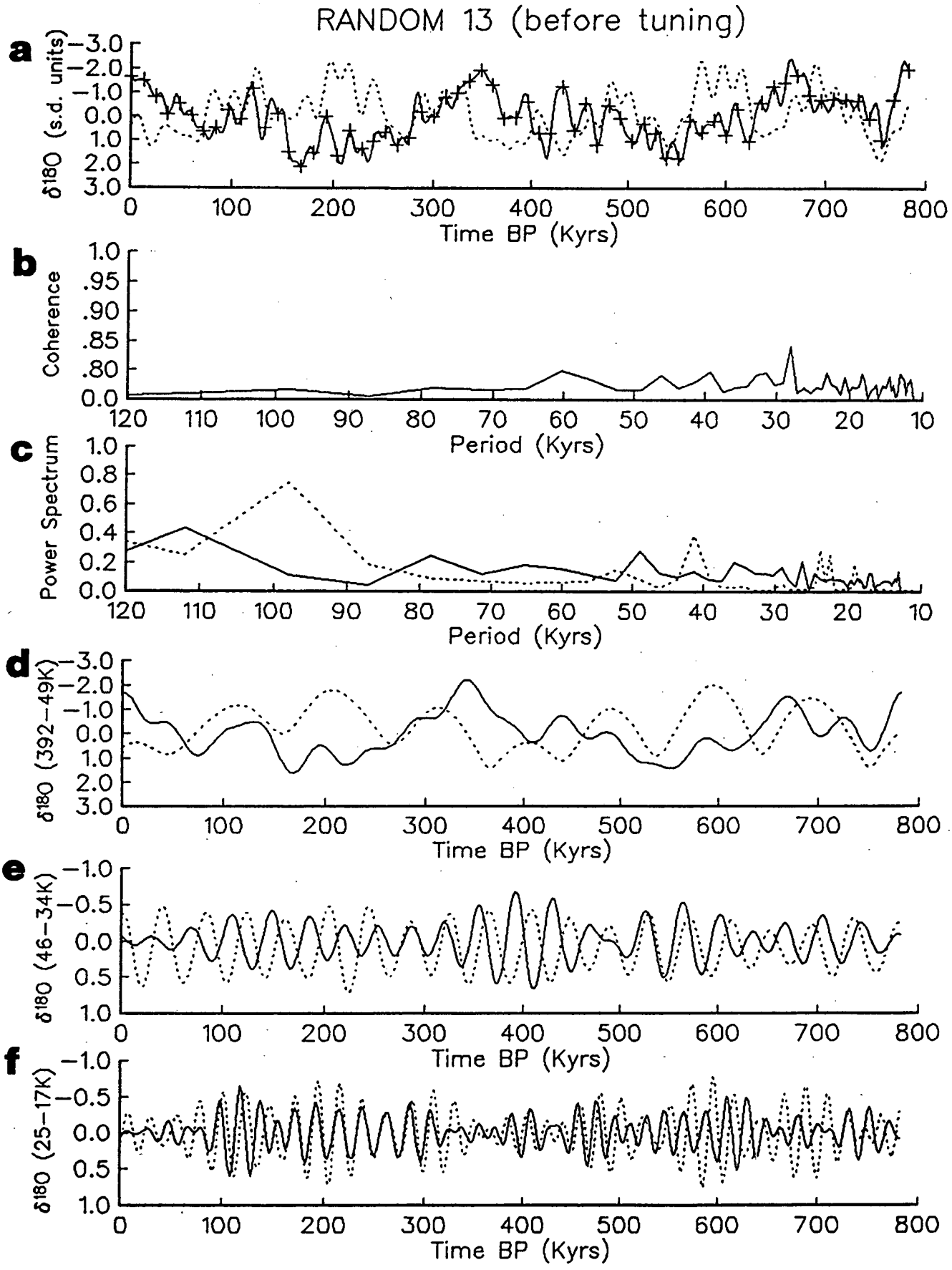
RANDOM 13 (before tuning)
a
δ18O (s.d. units)
−3.0
−2.0
−1.0
0.0
1.0
2.0
3.0
0
100
200
300
400
500
600
700
800
Time BP (Kyrs)
b
Coherence
1.0
.95
.90
.85
.80
0.0
120
110
100
90
80
70
60
50
40
30
20
10
Period (Kyrs)
c
Power Spectrum
1.0
0.8
0.6
0.4
0.2
0.0
120
110
100
90
80
70
60
50
40
30
20
10
Period (Kyrs)
d
δ18O (392−49K)
−3.0
−2.0
−1.0
0.0
1.0
2.0
3.0
0
100
200
300
400
500
600
700
800
Time BP (Kyrs)
e
δ18O (46−34K)
−1.0
−0.5
0.0
0.5
1.0
0
100
200
300
400
500
600
700
800
Time BP (Kyrs)
f
δ18O (25−17K)
−1.0
−0.5
0.0
0.5
1.0
0
100
200
300
400
500
600
700
800
Time BP (Kyrs)

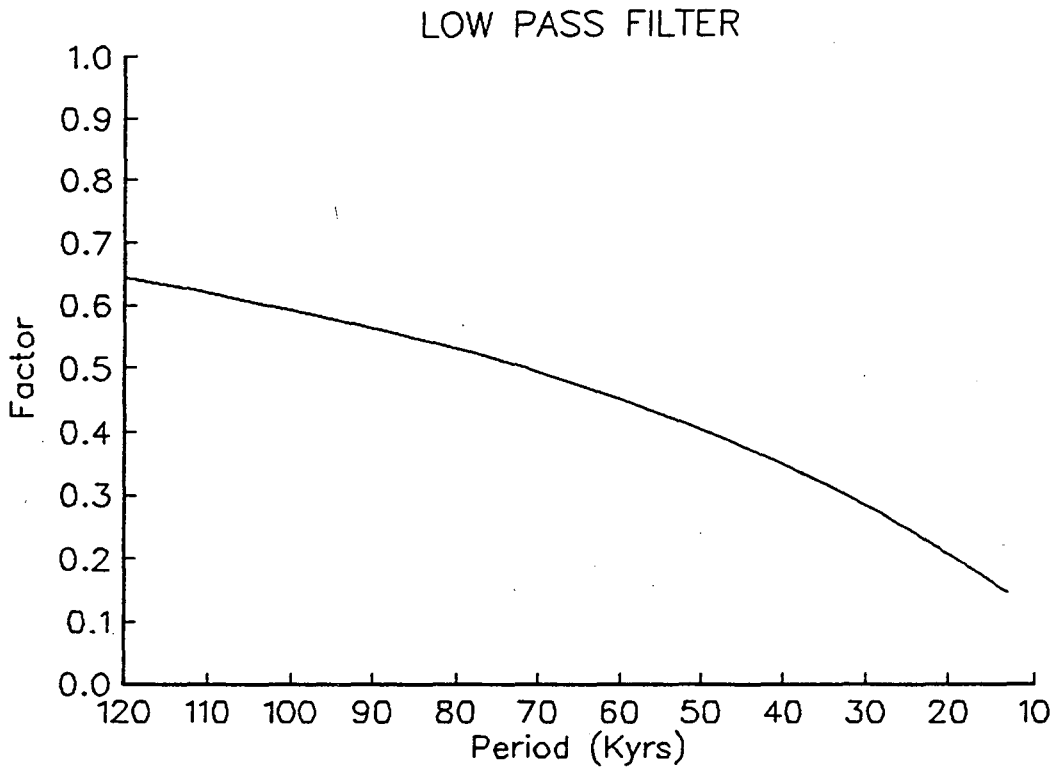
LOW PASS FILTER
Factor
1.0
0.9
0.8
0.7
0.6
0.5
0.4
0.3
0.2
0.1
0.0
120
110
100
90
80
70
60
50
40
30
20
10
Period (Kyrs)

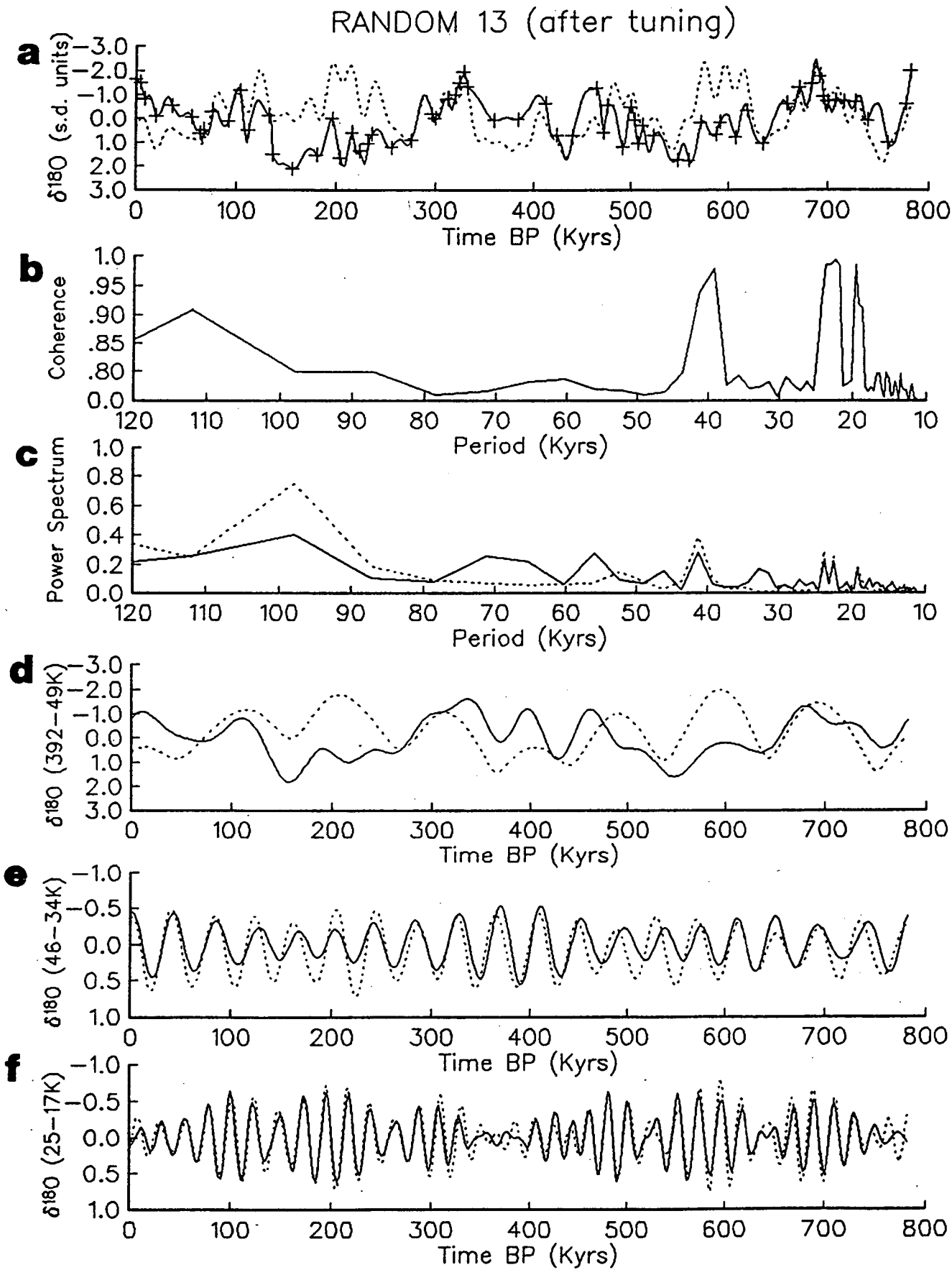
RANDOM 13 (after tuning)
a
δ18O (s.d. units)
Time BP (Kyrs)
b
Coherence
Period (Kyrs)
c
Power Spectrum
Period (Kyrs)
d
δ18O (392–49K)
Time BP (Kyrs)
e
δ18O (46–34K)
Time BP (Kyrs)
f
δ18O (25–17K)
Time BP (Kyrs)

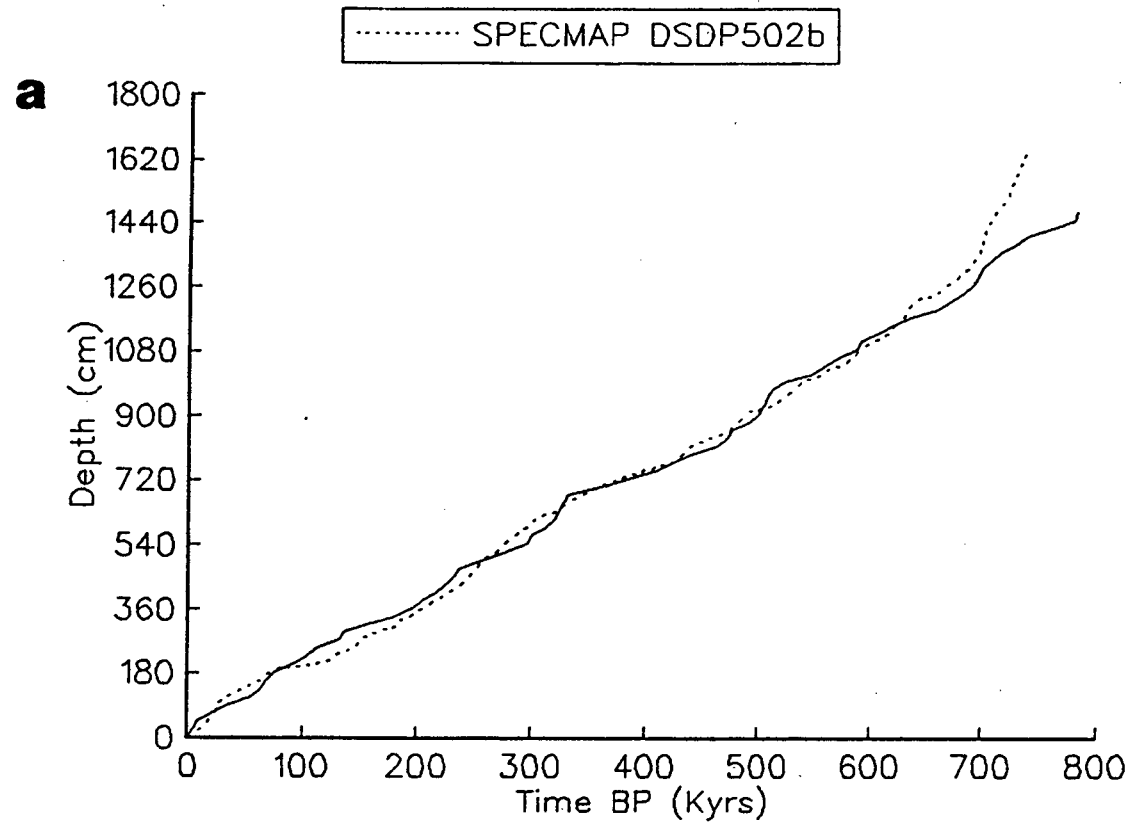
SPECMAP DSDP502b
a
1800
1620
1440
1260
1080
900
720
540
360
180
0
Depth (cm)
0
100
200
300
400
500
600
700
800
Time BP (Kyrs)

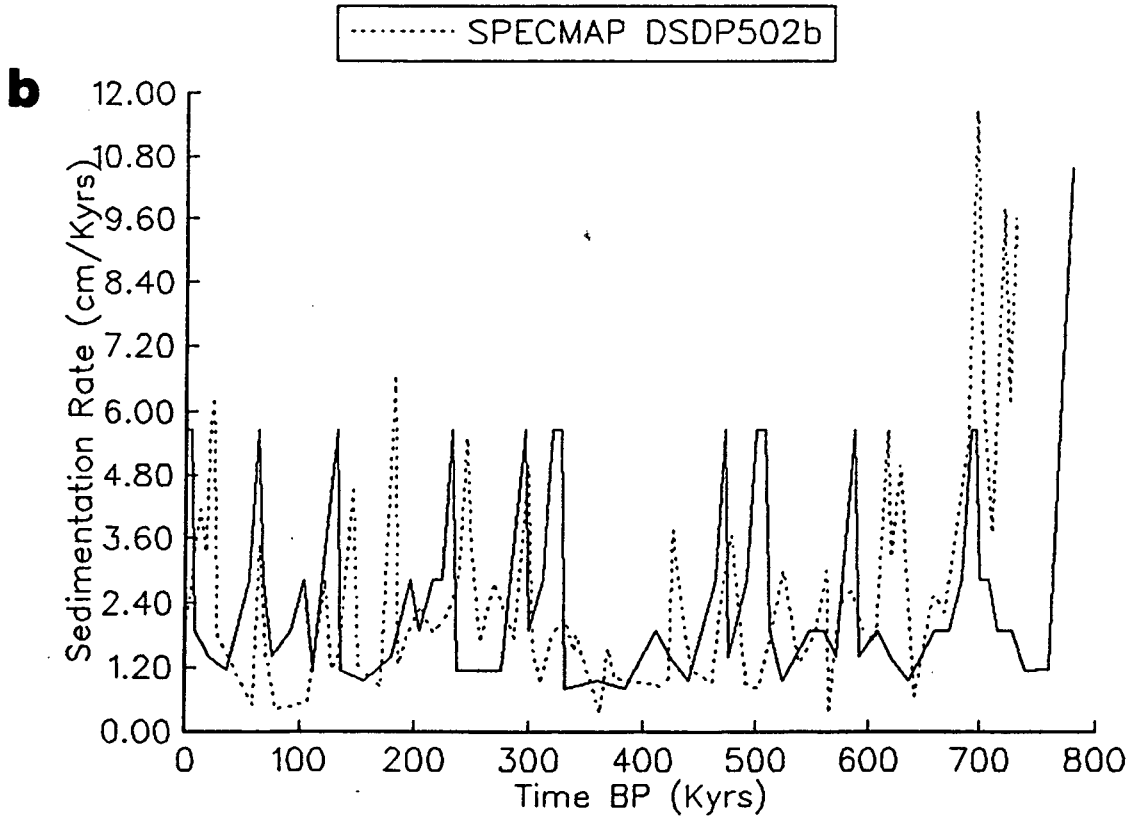
SPECMAP DSDP502b
b
12.00
10.80
9.60
8.40
7.20
6.00
4.80
3.60
2.40
1.20
0.00
Sedimentation Rate (cm/Kyrs)
0
100
200
300
400
500
600
700
800
Time BP (Kyrs)

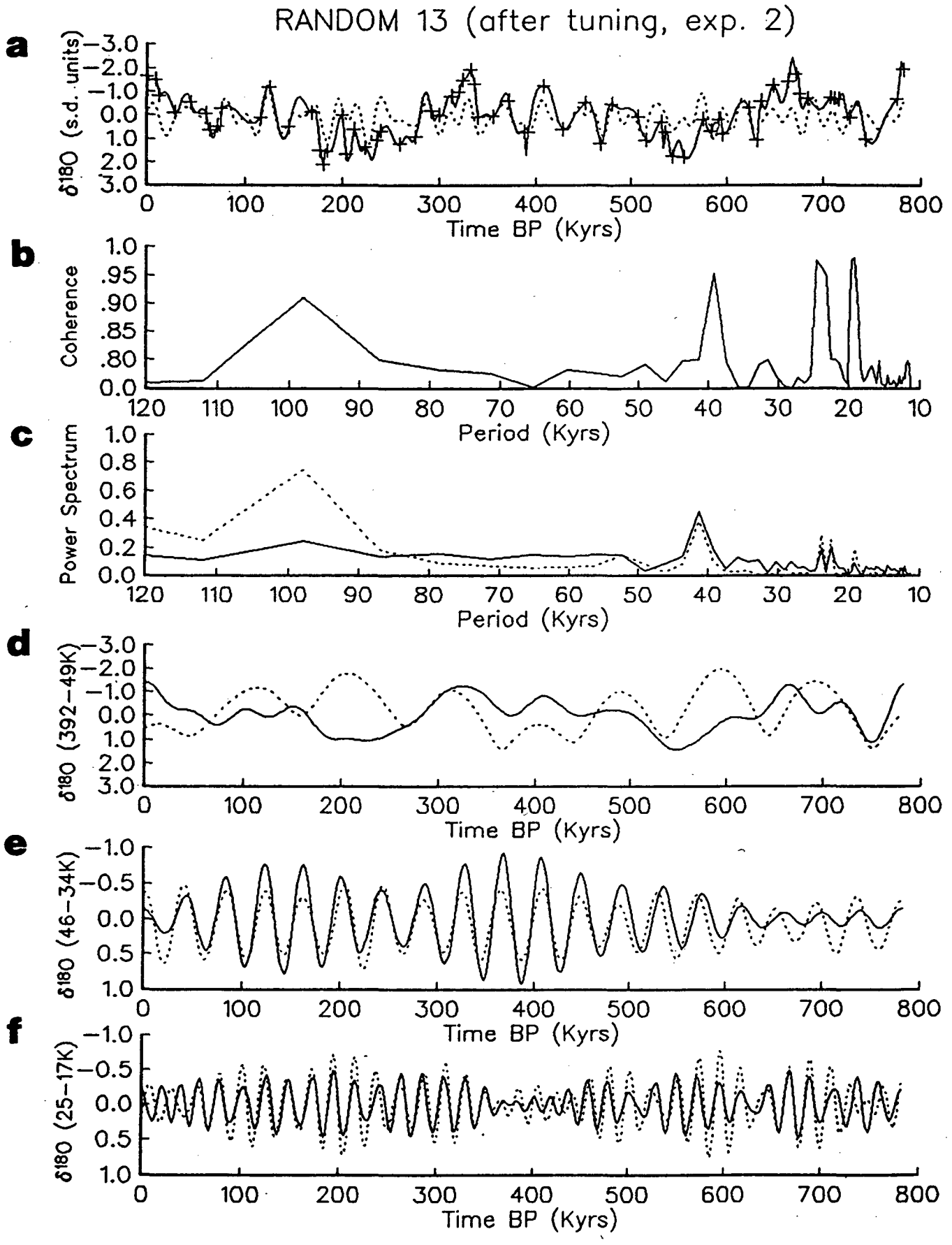
RANDOM 13 (after tuning, exp. 2)
a
δ18O (s.d. units)
−3.0
−2.0
−1.0
0.0
1.0
2.0
3.0
0 100 200 300 400 500 600 700 800
Time BP (Kyrs)
b
Coherence
1.0
.95
.90
.85
.80
0.0
120 110 100 90 80 70 60 50 40 30 20 10
Period (Kyrs)
c
Power Spectrum
1.0
0.8
0.6
0.4
0.2
0.0
120 110 100 90 80 70 60 50 40 30 20 10
Period (Kyrs)
d
δ18O (392−49K)
−3.0
−2.0
−1.0
0.0
1.0
2.0
3.0
0 100 200 300 400 500 600 700 800
Time BP (Kyrs)
e
δ18O (46−34K)
−1.0
−0.5
0.0
0.5
1.0
0 100 200 300 400 500 600 700 800
Time BP (Kyrs)
f
δ18O (25−17K)
−1.0
−0.5
0.0
0.5
1.0
0 100 200 300 400 500 600 700 800
Time BP (Kyrs)

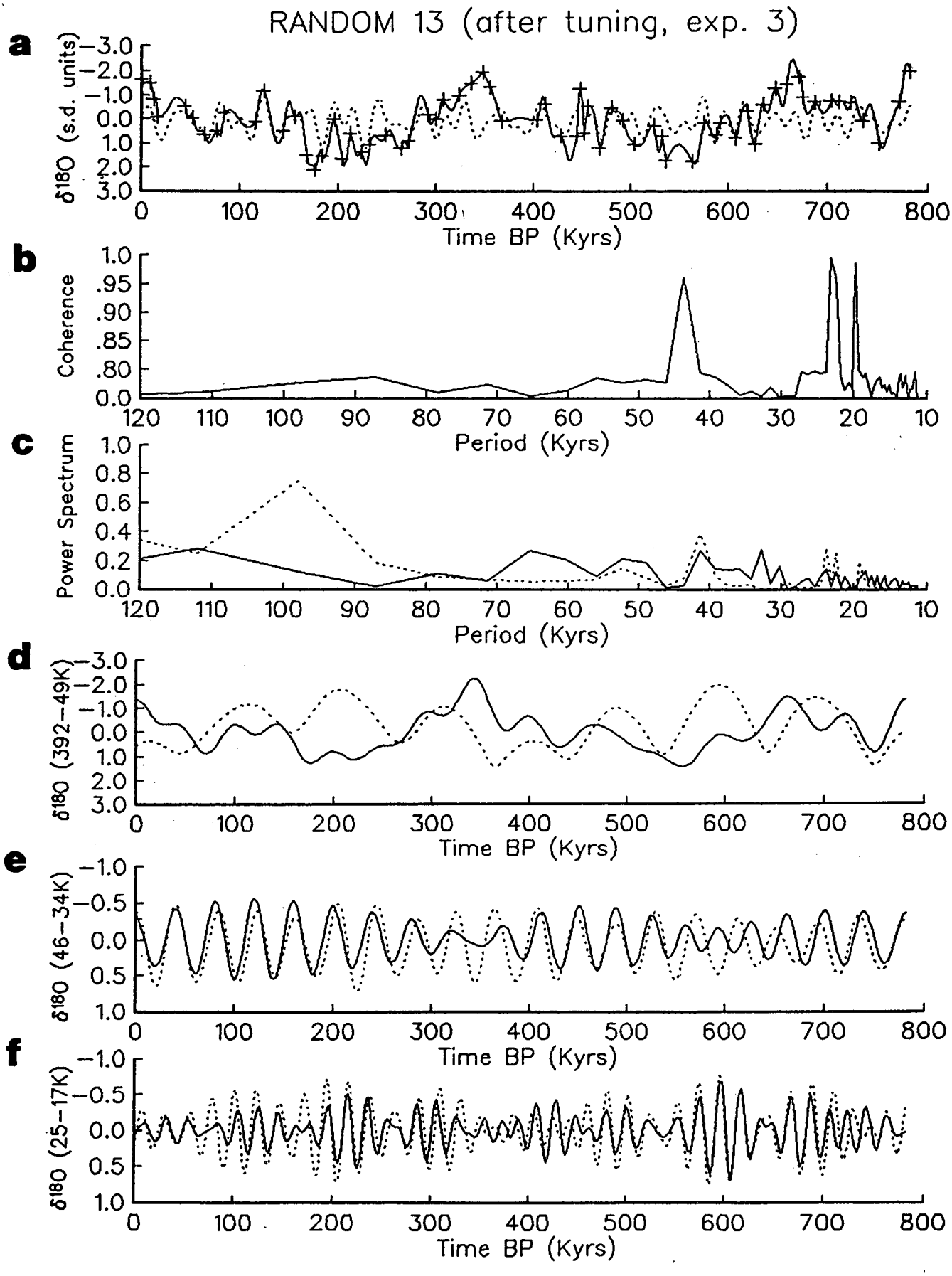
RANDOM 13 (after tuning, exp. 3)
a
δ18O (s.d. units)
−3.0
−2.0
−1.0
0.0
1.0
2.0
3.0
0
100
200
300
400
500
600
700
800
Time BP (Kyrs)
b
Coherence
1.0
.95
.90
.85
.80
0.0
120
110
100
90
80
70
60
50
40
30
20
10
Period (Kyrs)
c
Power Spectrum
1.0
0.8
0.6
0.4
0.2
0.0
120
110
100
90
80
70
60
50
40
30
20
10
Period (Kyrs)
d
δ18O (392−49K)
−3.0
−2.0
−1.0
0.0
1.0
2.0
3.0
0
100
200
300
400
500
600
700
800
Time BP (Kyrs)
e
δ18O (46−34K)
−1.0
−0.5
0.0
0.5
1.0
0
100
200
300
400
500
600
700
800
Time BP (Kyrs)
f
δ18O (25−17K)
−1.0
−0.5
0.0
0.5
1.0
0
100
200
300
400
500
600
700
800
Time BP (Kyrs)

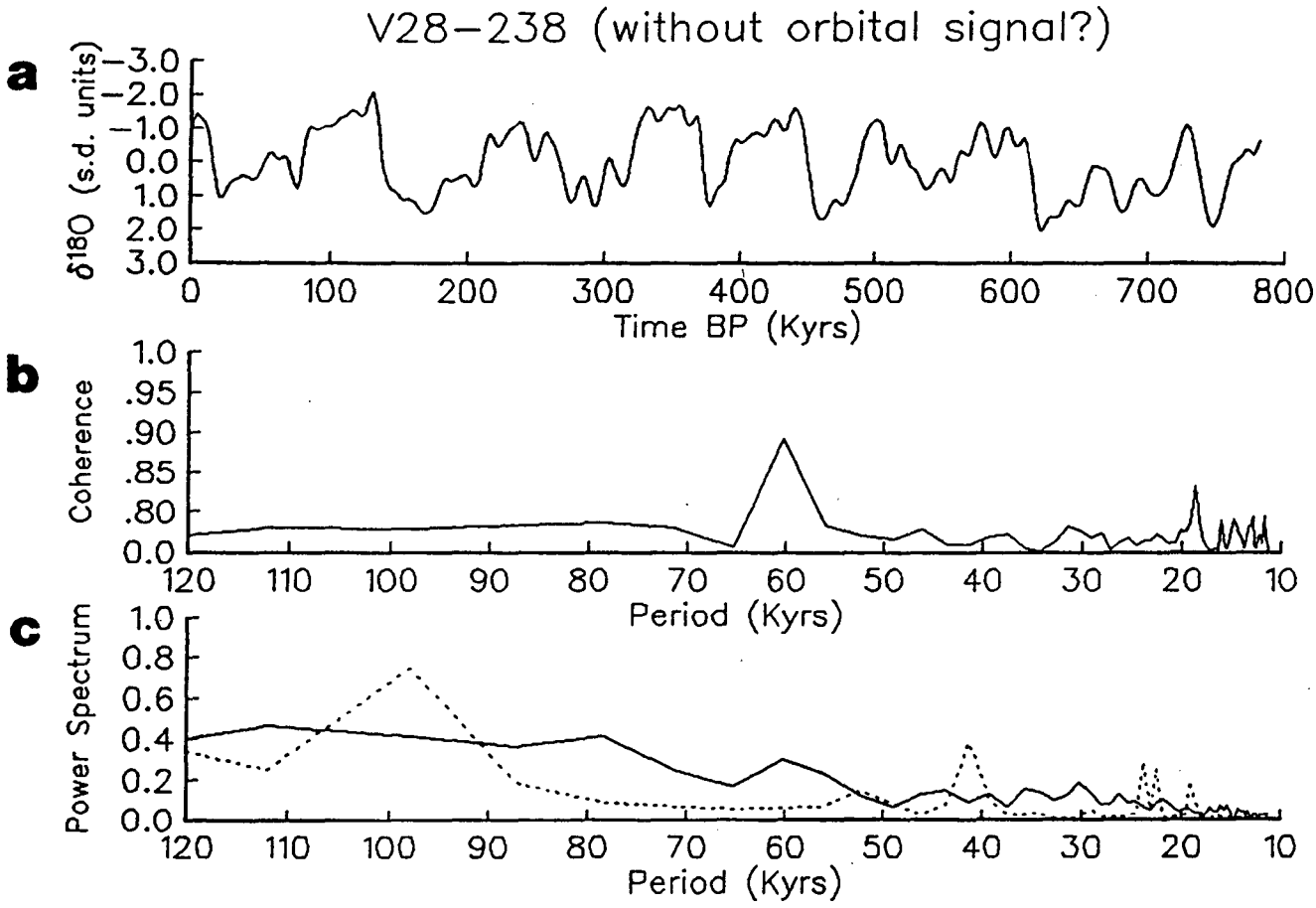
V28−238 (without orbital signal?)
a
δ18O (s.d. units)
−3.0
−2.0
−1.0
0.0
1.0
2.0
3.0
0
100
200
300
400
500
600
700
800
Time BP (Kyrs)
b
Coherence
1.0
.95
.90
.85
.80
0.0
120
110
100
90
80
70
60
50
40
30
20
10
Period (Kyrs)
c
Power Spectrum
1.0
0.8
0.6
0.4
0.2
0.0
120
110
100
90
80
70
60
50
40
30
20
10
Period (Kyrs)

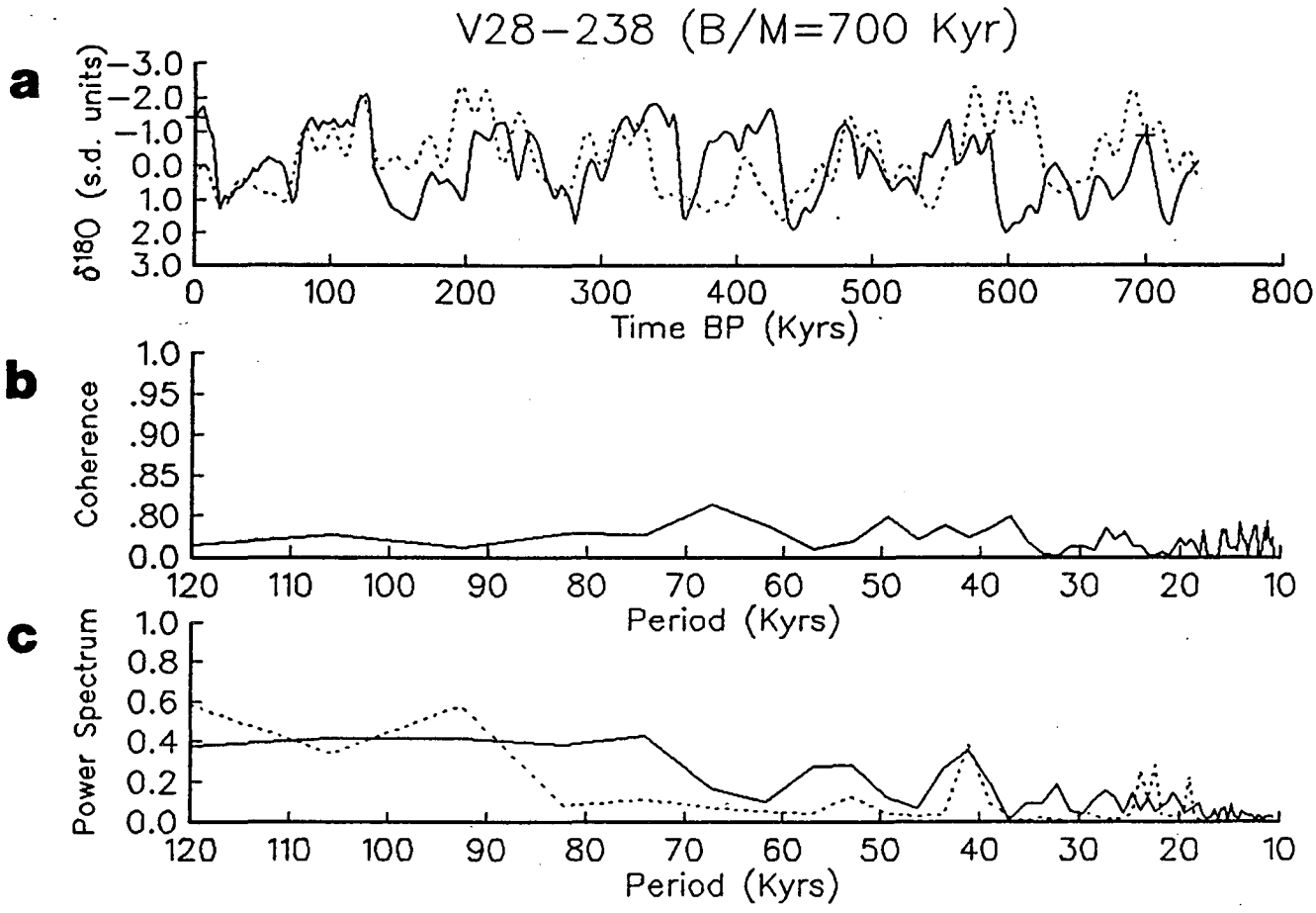
V28-238 (B/M=700 Kyr)
a
δ18O (s.d. units)
−3.0
−2.0
−1.0
0.0
1.0
2.0
3.0
0
100
200
300
400
500
600
700
800
Time BP (Kyrs)
b
Coherence
1.0
.95
.90
.85
.80
0.0
120
110
100
90
80
70
60
50
40
30
20
10
Period (Kyrs)
c
Power Spectrum
1.0
0.8
0.6
0.4
0.2
0.0
120
110
100
90
80
70
60
50
40
30
20
10
Period (Kyrs)

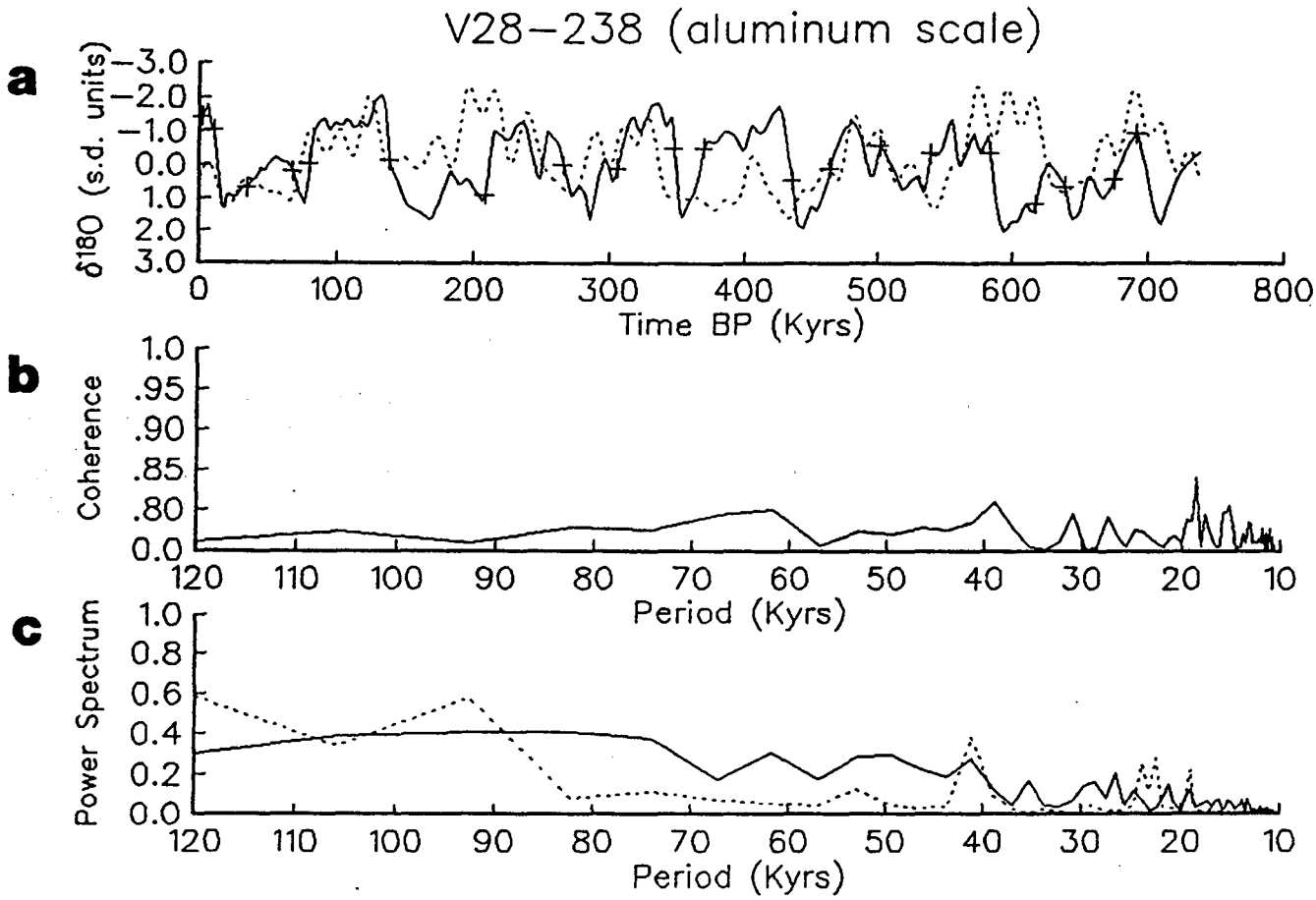
V28−238 (aluminum scale)
a
δ18O (s.d. units)
−3.0
−2.0
−1.0
0.0
1.0
2.0
3.0
0
100
200
300
400
500
600
700
800
Time BP (Kyrs)
b
Coherence
1.0
.95
.90
.85
.80
0.0
120
110
100
90
80
70
60
50
40
30
20
10
Period (Kyrs)
c
Power Spectrum
1.0
0.8
0.6
0.4
0.2
0.0
120
110
100
90
80
70
60
50
40
30
20
10
Period (Kyrs)

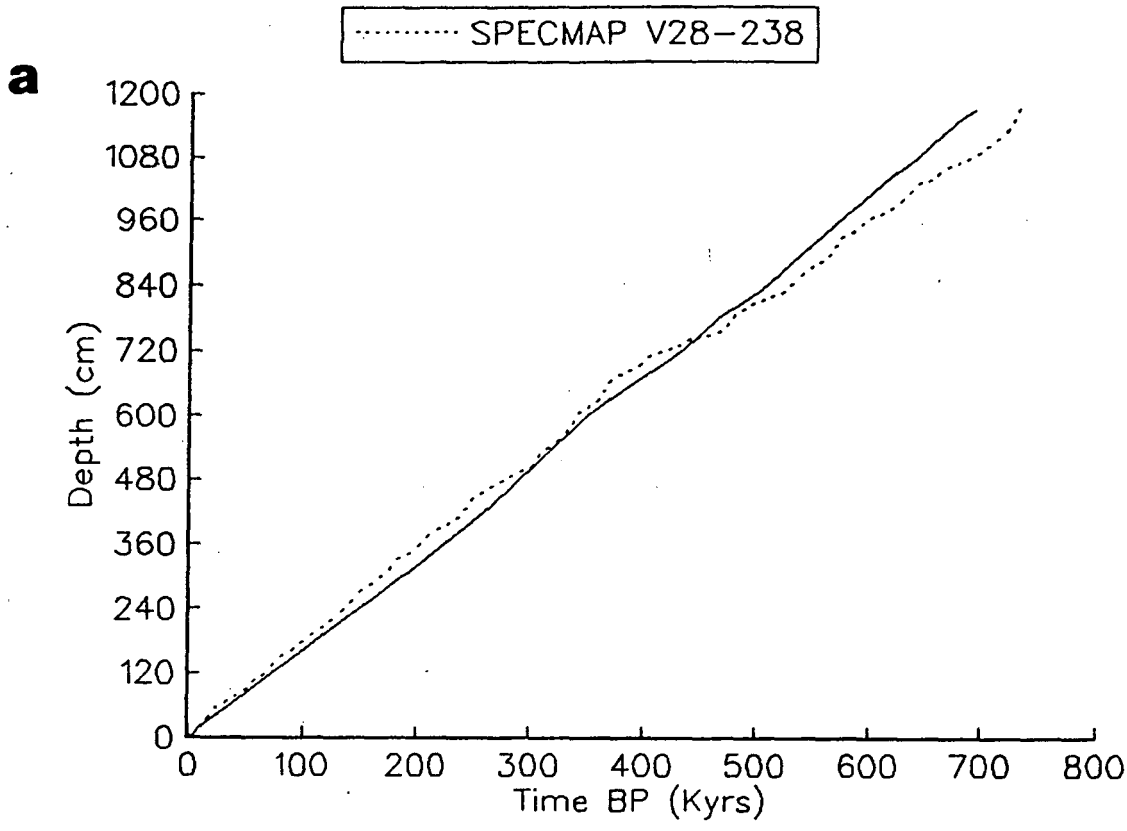
a
SPECMAP V28-238
Depth (cm)
1200
1080
960
840
720
600
480
360
240
120
0
0
100
200
300
400
500
600
700
800
Time BP (Kyrs)

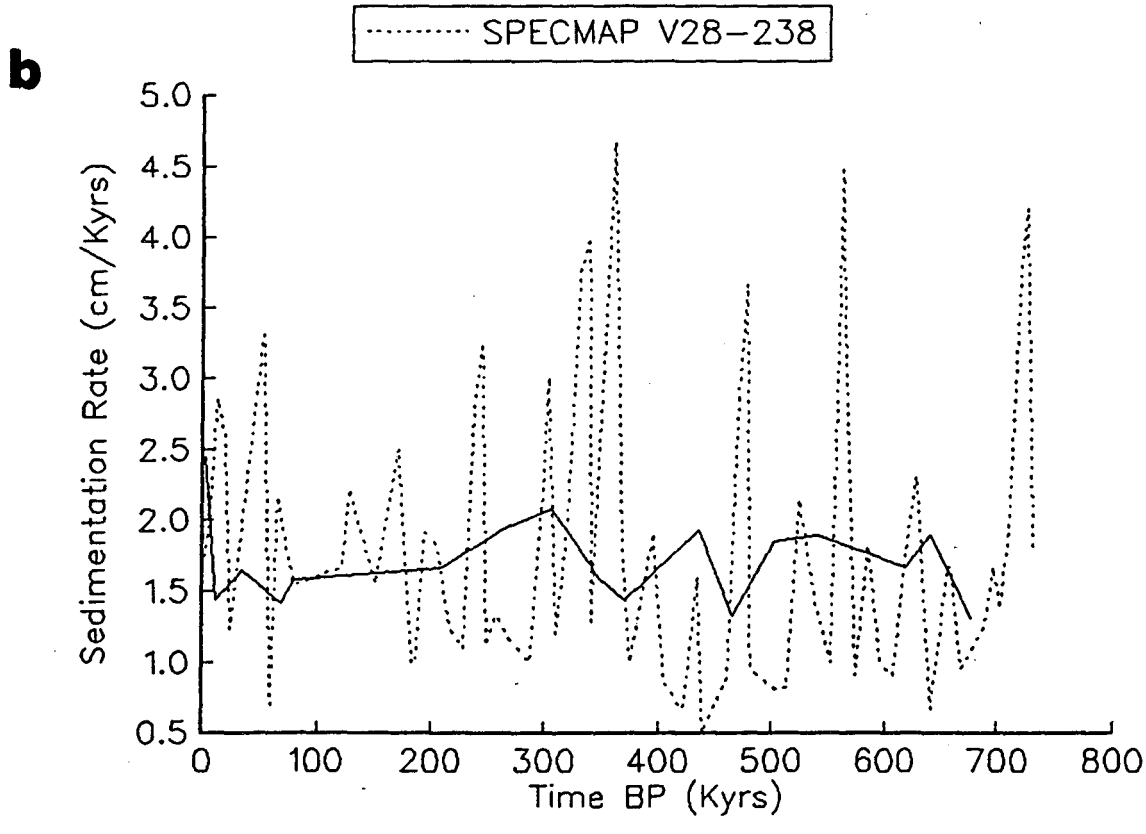
b
SPECMAP V28-238
Sedimentation Rate (cm/Kyrs)
5.0
4.5
4.0
3.5
3.0
2.5
2.0
1.5
1.0
0.5
0
100
200
300
400
500
600
700
800
Time BP (Kyrs)

TABLE 1. The spectrum of significant coherencies (>0.75) and their phases for the SPECMAP stack.

Period (Kyr)	Coherence	Phase (degrees)
98.0	0.77	15
87.1	0.97	8
60.3	0.84	44
43.6	0.92	-2
41.3	0.92	1
39.2	0.87	1
25.3	0.80	27
24.5	0.98	20
23.8	0.97	21
23.1	0.97	23
22.4	0.90	28
21.8	0.88	27
21.2	0.78	57
20.1	0.88	30
19.6	0.92	-15
19.1	0.93	-16
18.7	0.90	-18
11.4	0.93	-154

TABLE 2. The spectrum of significant coherencies (>0.75) and their phases for the tuned RANDOM 13 curve (first experiment, Fig. 7).

Period (Kyr)	Coherence	Phase (degrees)
112.0	0.91	7
98.0	0.79	11
87.1	0.77	8
43.6	0.76	-23
41.3	0.94	-22
39.2	0.98	-21
24.5	0.88	-9
23.8	0.98	-9
23.1	0.98	-4
22.4	0.99	2
21.8	0.98	2
19.6	0.99	5
19.1	0.92	3
18.7	0.91	5
15.4	0.76	-37

Ernest Orlando Lawrence Berkeley National Laboratory
One Cyclotron Road | Berkeley, California 94720

Prepared for the U.S. Department of Energy under Contract No. DE-AC03-76SF00098